OUTP-11-49P

New Physics in Γ_{12}^s: $(\bar{s}b)(\bar{\tau}\tau)$ Operators

Christoph Bobeth[a] and Ulrich Haisch[b]

[a]*Institute for Advanced Study and Excellence Cluster Universe*
Technische Universität München
D-85748 Garching, Germany

[b]*Rudolf Peierls Centre for Theoretical Physics*
University of Oxford
OX1 3PN Oxford, United Kingdom

arXiv:1109.1826v4 [hep-ph] 26 Nov 2013

Abstract

Measurements performed at the Tevatron of both the like-sign dimuon charge asymmetry in $B_{d,s}$-meson samples and the mixing-induced CP asymmetry in $B_s \to J/\psi\phi$ depart from their standard model (SM) predictions. This could be an indication for new CP phases in $\Delta B = 2$ transitions, preferentially in B_s–$\bar{B}_s$ mixing. The experimental situation, however, remained inconclusive, as it favored values of the element Γ_{12}^s of the decay matrix in the B_s-meson system that are notably different from the SM expectation, suggesting the presence of new physics in the $\Delta B = 1$ sector as well. The very recent LHCb measurements of $B_s \to J/\psi\phi$ and $B_s \to J/\psi f_0$, which do not find any evidence for a new-physics phase in the element M_{12}^s of the mass matrix, point into this direction as well. In this article, we explore the potential size of non-standard effects in Γ_{12}^s stemming from dimension-six operators with flavor content $(\bar{s}b)(\bar{\tau}\tau)$. We show that since the existing constraints imposed by tree- and loop-level mediated $B_{d,s}$-meson decays are quite loose, the presence of absorptive new physics of this type would lead to an improved global fit to the current data. The allowed effects are however far too small to provide a full explanation of the observed anomalies. Our model-independent conclusions are finally contrasted with explicit analyses of the new-physics effects in B_s–$\bar{B}_s$ mixing that can arise from leptoquarks or Z' bosons.

Contents

1 Introduction **1**

2 Preliminaries **8**

3 Direct Bounds on $(\bar{s}b)(\bar{\tau}\tau)$ Operators **9**

4 Indirect Bounds on $(\bar{s}b)(\bar{\tau}\tau)$ Operators **13**

5 Effects of $(\bar{s}b)(\bar{\tau}\tau)$ Operators in Γ_{12}^s **19**

6 New-Physics Models **22**

7 Summary **28**

A Operator Mixing **30**

B Kinematic Functions **31**

C Matrix Elements for $b \to s\ell^+\ell^-$ **32**

D Matrix Elements for $b \to s\gamma\gamma$ **33**

E Forward-Scattering Amplitudes **35**

F Bounds on $\Delta\Gamma_s$ and a_{fs}^s from ΔM_s **36**

1 Introduction

The phenomenon of neutral B_s-meson mixing is encoded in the off-diagonal elements M_{12}^s and Γ_{12}^s of the mass and decay rate matrix. These two complex parameters can be fully determined by measuring the mass difference $\Delta M_s = M_H^s - M_L^s$, the CP-violating phase $\phi_{J/\psi\phi}^s = -2\beta_s$, the decay width difference $\Delta\Gamma_s = \Gamma_L^s - \Gamma_H^s$, and the CP asymmetry a_{fs}^s in flavor-specific decays.

The combined Tevatron and LHC determination of the mass difference reads [1, 2]

$$\Delta M_s = (17.73 \pm 0.05)\,\text{ps}^{-1}\,, \tag{1}$$

and agrees well with the corresponding standard model (SM) prediction [3]

$$(\Delta M_s)_{\text{SM}} = (17.3 \pm 2.6)\,\text{ps}^{-1}\,. \tag{2}$$

Here the quoted errors correspond to 68% confidence level (CL) ranges.

The phase difference $\phi_{J/\psi\phi}^s$ between the B_s mixing and the $b \to sc\bar{c}$ decay amplitude and the width difference $\Delta\Gamma_s$ can be simultaneously determined from an analysis of the flavor-tagged time-dependent decay $B_s \to J/\psi\phi$. The 2010 HFAG average[1] combines the results of

[1]Notice that only results published or accepted in a refereed journal by March 15, 2011 have been included in the average.

CDF [4, 5] and DØ [6], which are based on $1.35\,\text{fb}^{-1}$ and $2.8\,\text{fb}^{-1}$ of $p\bar{p}$ data at $\sqrt{s} = 1.96$ TeV, respectively. At 68% CL they find [7]

$$\phi^s_{J/\psi\phi} = \left(-44^{+17}_{-21}\right)^\circ\,, \qquad \Delta\Gamma_s = \left(0.154^{+0.054}_{-0.070}\right)\text{ps}^{-1}\,, \tag{3}$$

as well as a symmetric solution located at $180^\circ - \phi^s_{J/\psi\phi}$ and $-\Delta\Gamma_s$.[2] The corresponding numbers in the SM are [3, 9][3]

$$(\phi^s_{J/\psi\phi})_{\text{SM}} = \arg\left[\frac{(V^*_{ts}V_{tb})^2}{(V^*_{cs}V_{cb})^2}\right] = (-2.1 \pm 0.1)^\circ\,, \qquad (\Delta\Gamma_s)_{\text{SM}} = (0.087 \pm 0.021)\,\text{ps}^{-1}\,. \tag{4}$$

They deviate from (3) by 2.3σ and 0.9σ, respectively.

Meanwhile, CDF, DØ, and LHCb provided new measurements of $\phi^s_{J/\psi\phi}$ and $\Delta\Gamma_s$ with data from 2011 which have been combined in the new HFAG 2012 release [11]. Both, the CDF [12] and DØ [13] collaborations, have upgraded their $B_s \to J/\psi\phi$ analysis to integrated luminosities of $9.6\,\text{fb}^{-1}$ and $8.0\,\text{fb}^{-1}$, whereas LHCb analyzed $B_s \to J/\psi\phi$ [14] and $B_s \to J/\psi\pi^+\pi^-$ [15] using $1\,\text{fb}^{-1}$ of data. The combined results show no evidence for a new-physics phase in B_s–$\bar{B}_s$ mixing and a value for $\Delta\Gamma_s$ that is above the SM expectation (4), but compatible within the uncertainties.[4] The corresponding central values and 68% CL error ranges are

$$\phi^s_{J/\psi\phi} = \left(-2.5^{+5.2}_{-4.9}\right)^\circ\,, \qquad \Delta\Gamma_s = (0.105 \pm 0.015)\,\text{ps}^{-1}\,. \tag{5}$$

The CP asymmetry in flavor-specific decays a^s_{fs} can be extracted from a measurement of the like-sign dimuon charge asymmetry A^b_{SL}, which involves a sample that is almost evenly composed of B_d and B_s mesons. Performing a weighted average of the results by CDF [18] and DØ [19, 20], which are based on $1.6\,\text{fb}^{-1}$ and $6.1\,\text{fb}^{-1}$ of integrated luminosity (obtained before 2011), leads to

$$A^b_{\text{SL}} = (-8.5 \pm 2.8)\cdot 10^{-3}\,, \tag{6}$$

at 68% CL. Utilizing the SM predictions for the individual flavor-specific CP asymmetries [3]

$$(a^d_{fs})_{\text{SM}} = -(4.1 \pm 0.6)\cdot 10^{-4}\,, \qquad (a^s_{fs})_{\text{SM}} = (1.9 \pm 0.3)\cdot 10^{-5}\,, \tag{7}$$

one obtains

$$(A^b_{\text{SL}})_{\text{SM}} = (0.506 \pm 0.043)\,(a^d_{fs})_{\text{SM}} + (0.494 \pm 0.043)\,(a^s_{fs})_{\text{SM}} = (-2.0 \pm 0.4)\cdot 10^{-4}\,, \tag{8}$$

which differs from (6) by 3.0σ. Using the measured value of the CP asymmetry in flavor-specific B_d decays [7],[5]

$$a^d_{fs} = (-4.7 \pm 4.6)\cdot 10^{-3}\,, \tag{9}$$

[2] The solution $180^\circ - \phi^s_{J/\psi\phi}$ and $-\Delta\Gamma_s$ has by now been excluded by LHCb at 4.7σ [8].

[3] A recent concise review of the theoretical uncertainties plaguing $(\Delta\Gamma_s)_{\text{SM}}$ has been given in [10].

[4] Very recently, the ATLAS collaboration has also presented measurements of $\phi^s_{J/\psi\phi}$ and $\Delta\Gamma_s$ [16] based on $4.9\,\text{fb}^{-1}$ of data. We add that the error of $\Delta\Gamma_s = (0.053 \pm 0.023)\,\text{ps}^{-1}$ reported by ATLAS is small, and that the quoted central value is below the SM prediction. These new results have not yet been included in the HFAG averages (5) that we will use in our work.

[5] The latest DØ measurement of a^d_{fs} yielding $a^d_{fs} = (6.8 \pm 4.7)\cdot 10^{-3}$ [17] is not considered here, because it is not incorporated in the official HFAG average presently.

and (6) in (8), one can also directly derive a value of a^s_{fs}. One arrives at

$$a^s_{fs} = (-1.2 \pm 0.7) \cdot 10^{-2} \,, \tag{10}$$

which compared to (7) represents a discrepancy of 1.7σ. Recently, the DØ collaboration has updated its analysis of the like-sign dimuon charge asymmetry. Employing $9.0\,\text{fb}^{-1}$ of data, they now find [21]

$$A^b_{\rm SL} = (-7.87 \pm 1.72_{\rm stat.} \pm 0.93_{\rm syst.}) \cdot 10^{-3} \,. \tag{11}$$

This new number should be confronted with the SM value

$$(A^b_{\rm SL})_{\rm SM} = (0.594 \pm 0.022)\,(a^d_{fs})_{\rm SM} + (0.406 \pm 0.022)\,(a^s_{fs})_{\rm SM} = (-2.4 \pm 0.4) \cdot 10^{-4} \,, \tag{12}$$

which corresponds to a tension with a statistical significance of 3.9σ. This result has been combined by HFAG [11] with the latest B-factory results on a^d_{fs} yielding

$$a^d_{fs} = (-3.3 \pm 3.3) \cdot 10^{-3} \,, \qquad a^s_{fs} = (-1.05 \pm 0.64) \cdot 10^{-2} \,. \tag{13}$$

Notice that the value for a^s_{fs} quoted above differs from $(a^s_{fs})_{\rm SM}$ as given in (7) by 1.6σ only. The average (13) does not take into account the latest LHCb measurement $a^s_{fs} = (-0.24 \pm 0.63) \cdot 10^{-2}$ [22] which is in agreement with the SM within uncertainties. Incorporating the latter number into a naive weighted average, results in $a^s_{fs} = (-0.64 \pm 0.45) \cdot 10^{-2}$, which corresponds to a tension of 1.4σ. It should be noted, that the combination of $A^b_{\rm SL}$ and a^d_{fs} in order to determine a^s_{fs} accounts for contributions beyond the SM which affect a^d_{fs}. When using instead the SM value of a^d_{fs}, the latest result of $A^b_{\rm SL}$ given in (11) implies $a^s_{fs} = (-1.88 \pm 0.49) \cdot 10^{-2}$, which deviates from the SM by 3.8σ, *i.e.*, a deviation of similar size as directly seen in $A^b_{\rm SL}$.

In view of the observed departures from the SM predictions, it is natural to ask what kind of new physics is able to simultaneously explain the observed values of ΔM_s, $\phi^s_{J/\psi\phi}$, $\Delta\Gamma_s$, and a^s_{fs}. Here we would like to address the found anomalies in a model-independent way by parametrizing the off-diagonal elements of the mass and decay rate matrix as follows

$$\begin{aligned} M^s_{12} &= (M^s_{12})_{\rm SM} + (M^s_{12})_{\rm NP} = (M^s_{12})_{\rm SM}\, R_M\, e^{i\phi_M} \,, \\ \Gamma^s_{12} &= (\Gamma^s_{12})_{\rm SM} + (\Gamma^s_{12})_{\rm NP} = (\Gamma^s_{12})_{\rm SM}\, R_\Gamma\, e^{i\phi_\Gamma} \,. \end{aligned} \tag{14}$$

In the presence of generic new physics, the B_s-meson observables of interest are then given to leading power in $|\Gamma^s_{12}|/|M^s_{12}|$ by

$$\begin{aligned} \Delta M_s &= (\Delta M_s)_{\rm SM}\, R_M \,, \qquad \phi^s_{J/\psi\phi} = (\phi^s_{J/\psi\phi})_{\rm SM} + \phi_M \,, \\ \Delta\Gamma_s &= (\Delta\Gamma_s)_{\rm SM}\, R_\Gamma\, \frac{\cos\left(\phi^s_{\rm SM} + \phi_M - \phi_\Gamma\right)}{\cos\phi^s_{\rm SM}} \approx (\Delta\Gamma_s)_{\rm SM}\, R_\Gamma\, \cos\left(\phi_M - \phi_\Gamma\right) \,, \\ a^s_{fs} &= (a^s_{fs})_{\rm SM}\, \frac{R_\Gamma}{R_M}\, \frac{\sin\left(\phi^s_{\rm SM} + \phi_M - \phi_\Gamma\right)}{\sin\phi^s_{\rm SM}} \approx (a^s_{fs})_{\rm SM}\, \frac{R_\Gamma}{R_M}\, \frac{\sin\left(\phi_M - \phi_\Gamma\right)}{\phi^s_{\rm SM}} \,. \end{aligned} \tag{15}$$

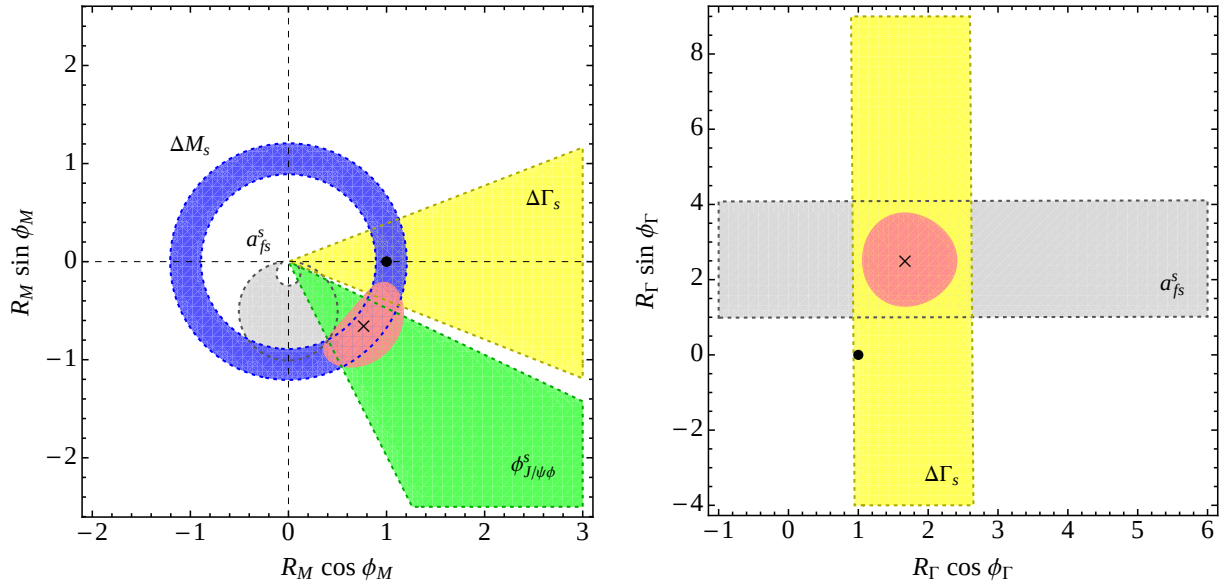


Figure 1: Left (Right): Constraints on the parameter R_M and ϕ_M (R_Γ and ϕ_Γ) from the global fit to the data set D1 in scenario S1 (S2). For the individual constraints the colored areas represent 68% CL regions (dofs = 1), while for the combined fit to the B_s-meson mixing data the light red area shows the 95% probability region (dofs = 2). In both panels the SM prediction (best-fit solution) is indicated by a dot (cross).

Notice that in the case of $\Delta\Gamma_s$ and a^s_{fs} the final results have been obtained by an expansion in $\phi^s_{\rm SM} = \arg\left(-(M^s_{12})_{\rm SM}/(\Gamma^s_{12})_{\rm SM}\right)$. Although this is an excellent approximation, given that $\phi^s_{\rm SM} = (0.22 \pm 0.06)^\circ$ [9], we will employ the exact analytic expressions in our numerical analysis.

The four real parameters $R_{M,\Gamma}$ and $\phi_{M,\Gamma}$ entering (14) can be constrained by confronting the observed values of ΔM_s, $\phi^s_{J/\psi\phi}$, $\Delta\Gamma_s$, and a^s_{fs} with their SM predictions. In the following, we will analyse two different data sets.[6] The first set (D1) consists out of (1), (3), and (10), while in the second case (D2), we rely on (1), (5), and (13). We begin our analysis by asking how well the SM hypothesis describes the two sets of data. In the case of D1, our global fit returns $\chi^2 = 9.1$ corresponding to 1.9σ (2.6σ) for 4 (2) degrees of freedom (dofs), while for D2 we obtain $\chi^2 = 3.2$, which translates into 0.6σ (1.3σ) if 4 (2) dofs are considered. One observes two features. First, the quality of the fit improves notably when going from D1 to D2, which is due to the fact that the value of $\phi^s_{J/\psi\phi}$ in the new data set is fully consistent with the SM expectation and, second, even the new data is not in perfect agreement with the SM hypothesis as a result of the observed large negative value of a^s_{fs} and, to a lesser extend, the latest measurement of $\Delta\Gamma_s$, which resides above the SM prediction. Let us also mention that using $A^b_{\rm SL}$ rather than a^s_{fs} in the χ^2 analysis (*i.e.*, fixing a^d_{fs} to its SM value and employing (6) instead of (10) in the case of D1 and (11) instead of (13) in the case of D2) would result in notable worse fits. One would find $\chi^2 = 14.6$ ($\chi^2 = 15.1$) for D1 (D2), corresponding to CL

[6]For simplicity we ignore the mirror solutions at $180^\circ - \phi^s_{J/\psi\phi}$ and $-\Delta\Gamma_s$ in our discussion hereafter.

values at or above the 3σ level. The χ^2 of the fit is in this case driven by $A^b_{\rm SL}$, which shows the largest deviations from the SM. Notice that employing the poor measurement of a^d_{fs} to extract a^s_{fs} from $A^b_{\rm SL}$, as done in (10) (and to less extend for (13) by HFAG [11]), while allowing to improve the fit to the B_s-meson data, comes of course with the price of a 1.0σ tension in a^d_{fs}. This feature should be clearly kept in mind when interpreting the CL levels quoted here and below.

It is also instructive to determine the best-fit solution of the full four-parameter fit to the data (1), (3), and (10) or (1), (5), and (13). In the case of D1, we find that $(R_M, \phi_M, R_\Gamma, \phi_\Gamma) = (1.02, -44^\circ, 3.1, 13^\circ)$ leads to a vanishing χ^2, while for D2 the χ^2 function equals zero at $(R_M, \phi_M, R_\Gamma, \phi_\Gamma) = (1.02, -0.4^\circ, 2.5, 61^\circ)$. After marginalization the corresponding symmetrized 68% CL parameter ranges are

$$\begin{aligned} R_M &= 1.05 \pm 0.16\,, & \phi_M &= (-46 \pm 19)^\circ\,, \\ R_\Gamma &= 3.3 \pm 1.5\,, & \phi_\Gamma &= (7 \pm 30)^\circ\,, \end{aligned} \tag{16}$$

and

$$\begin{aligned} R_M &= 1.05 \pm 0.16\,, & \phi_M &= (-0.4 \pm 5.2)^\circ\,, \\ R_\Gamma &= 2.6 \pm 1.2\,, & \phi_\Gamma &= (54 \pm 20)^\circ\,. \end{aligned} \tag{17}$$

We also note that the combination of $(a^d_{fs})_{\rm SM}$ with (11) in order to determine a^s_{fs} yields $(R_M, \phi_M, R_\Gamma, \phi_\Gamma) = (1.02, -0.4^\circ, 4.1, 73^\circ)$ and

$$\begin{aligned} R_M &= 1.05 \pm 0.16\,, & \phi_M &= (-0.4 \pm 5.2)^\circ\,, \\ R_\Gamma &= 4.2 \pm 1.2\,, & \phi_\Gamma &= (72 \pm 9)^\circ\,. \end{aligned} \tag{18}$$

Focusing on R_Γ and ϕ_G, we see that a good fit to the data sets requires very large corrections to Γ^s_{12}, either without (D1) or with (D2) a large weak phase. Even larger effects are required if one tries to explain (11) using $(a^d_{fs})_{\rm SM}$ as an input (a scenario that we will call D3 from hereon). Based on older data sets this observation has been made before in [23, 24, 25, 26] and triggered a considerable amount of theoretical investigations [27, 29, 28, 30, 31, 32, 33, 34]. The first publication that, to the best of our knowledge, argued convincingly for the possibility to have sizable new-physics effects in Γ^s_{12} is the work [35].

To further elucidate the latter point, we analyse two orthogonal hypothesis of new physics in B_s–$\bar{B}_s$ oscillations, namely a scenario with $(M^s_{12})_{\rm NP} \neq 0$ and $(\Gamma^s_{12})_{\rm NP} = 0$ and a scenario with $(M^s_{12})_{\rm NP} = 0$ and $(\Gamma^s_{12})_{\rm NP} \neq 0$. We refer to this two different scenarios as S1 and S2, respectively. The left (right) panel in Figure 1 shows the results of our global fit for scenario S1 (S2) in the $R_M \cos\phi_M$–$R_M \sin\phi_M$ ($R_\Gamma \cos\phi_\Gamma$–$R_\Gamma \sin\phi_\Gamma$) plane based on the data set D1. By inspection of the left plot, we infer that in the scenario S1 the preferred 95% CL parameter region, is essentially determined by the interplay of ΔM_s and $\phi^s_{J/\psi\phi}$. The best-fit point is located at $(R_M, \phi_M) = (1.01, -40^\circ)$. It has $\chi^2/{\rm dofs} = 3.1/2$ corresponding to 1.3σ,[7] which is in almost equal parts due to $\Delta\Gamma_s$ and a^s_{fs}. This moderate tension is also clearly visible in the figure. Turning our attention to the right panel, we observe that in the case of the hypothesis

[7] This result agrees well with the global analysis performed in [9], but disagrees with the work [33], which claims that the scenario S1 is disfavored by more than 3σ.

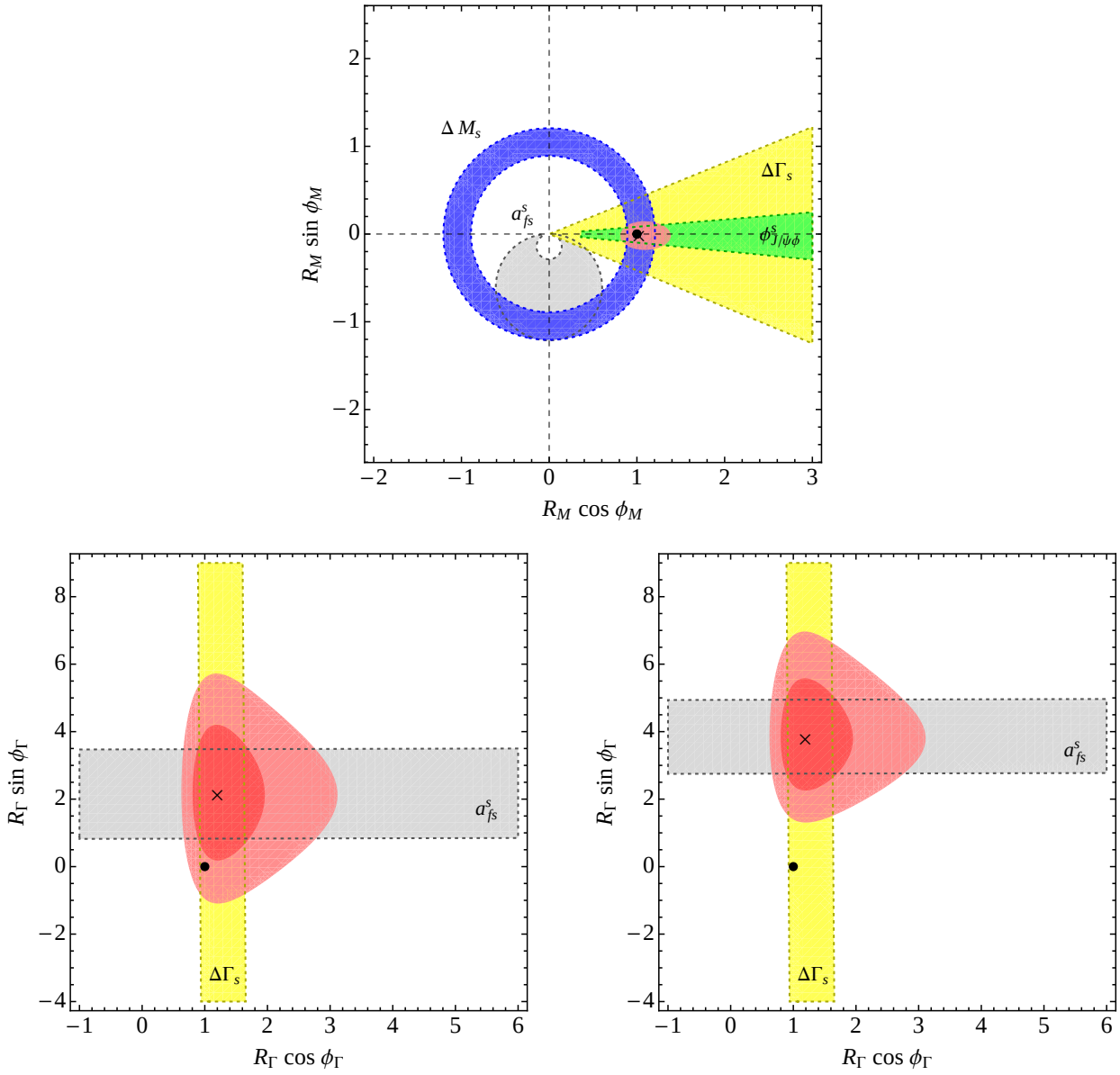


Figure 2: Upper (Lower left, right): Constraints on the parameter R_M and ϕ_M (R_Γ and ϕ_Γ) from the global fit to the data set D2 in scenario S1 (D2 in scenario S2, D3 in scenario S2). For the individual constraints the colored areas represent 68% CL regions (dofs = 1), while for the combined fit to the B_s-meson mixing data the red (light red) area shows the 68% (95%) probability region (dofs = 2). In all panels the SM prediction (best-fit solution) is indicated by a dot (cross).

S2 only a small region of parameter space has a CL that is better than 95%. The best-fit solution resides at $(R_\Gamma, \phi_\Gamma) = (3.0, 56^\circ)$ and has $\chi^2/\text{dofs} = 5.4/2$ corresponding to 1.8σ. These numbers imply that the data set D1 prefers the hypothesis S1 over S2.

By repeating the above statistical analysis for the new data set D2, we obtain the results

displayed in the upper and lower left panel in Figure 2. From the upper panel, we glean that in the scenario S1 the regions of all individual constraints apart from a_{fs}^s now overlap. Minimizing the χ^2 function gives $(R_M, \phi_M) = (1.02, -1.0^\circ)$ and $\chi^2/\text{dofs} = 3.2/2$ corresponding to 1.3σ, which represents only a marginal improvement with respect to the SM hypothesis. In consequence, the case for a non-zero non-standard contribution to M_{12}^s is rather weak. Comparing the right panel of Figure 1 with the lower left panel of Figure 2, we see that the 95% CL region is not only significantly larger in the scenario S2 than before, but that now also a description of the data with a probability of better than 68% is possible. The best-fit point is located at $(R_\Gamma, \phi_\Gamma) = (2.4, 61^\circ)$. In fact, the latter parameters lead to an almost perfect fit with $\chi^2/\text{dofs} = 0.03/2$ corresponding to 0.02σ. The new data set D2 hence statistically favors the new-physics scenario S2 over the hypothesis S1. We stress again that the best-fit points and CL values given in this and the last paragraph do depend on whether a_{fs}^s or $A_{\rm SL}^b$ is part of the χ^2 function. In particular, even larger values for R_Γ of around 4 would be needed to give a good fit in scenario S2, if (6) instead of (10) or (11) instead of (13) would been used. This feature is illustrated in the lower right panel in Figure 2, which shows the results of a fit to the data set D3.

The above findings suggest that one hypothetical explanation of the experimentally observed large negative values of a_{fs}^s (or equivalent $A_{\rm SL}^b$) consists in postulating new physics in Γ_{12}^s that changes the SM value by a factor of 3 or more. The goal of our work is to study in detail whether or not and to which extend such an speculative option is viable. While in principle any composite operator $(\bar{s}b)f$, with f leading to an arbitrary flavor neutral final state of at least two fields and total mass below the B_s-meson mass, can contribute to Γ_{12}^s, the field content of f is in practice very restricted, since $B_s \to f$ and $B_d \to X_s f$ decays to most final states involving light particles are severely constrained. One notable exception is the subclass of B_s- and B_d-meson decays to a pair of tau leptons [23, 26, 29, 30, 33, 35, 36], to which we will devote our full attention in this article. Specifically, we perform a thorough model-independent analysis of the impact of the complete set of $(\bar{s}b)(\bar{\tau}\tau)$ operators on Γ_{12}^s, taking into account all existing direct and indirect constraints. We find that the loose bounds on most of the Wilson coefficients of the considered operators allow for enhancements of Γ_{12}^s of maximal 35% compared to its SM value, but that the 300% effects in R_Γ needed to fully accommodate the data (see (16) and (17)) can clearly not be obtained. The presence of $(\bar{s}b)(\bar{\tau}\tau)$ operators alone can thus not reconcile the observed tensions in the $B_{d,s}$-meson data. Our work clarifies and extends the existing analyses [23, 29, 35]. While most of our discussion is based on an effective-field theory and thus general, we also consider two explicit models of new physics that alter Γ_{12}^s, namely leptoquarks and scenarios with new neutral gauge bosons.

This article is organized as follows. After introducing important definitions and notations in Section 2, we study in Section 3 the direct bounds on the Wilson coefficients of the $(\bar{s}b)(\bar{\tau}\tau)$ operators following from $B_s \to \tau^+\tau^-$, $B \to X_s\tau^+\tau^-$, and $B^+ \to K^+\tau^+\tau^-$. Section 4 is devoted to a comprehensive discussion of the indirect constraints arising from $b \to s\gamma$, $b \to s\ell^+\ell^-$ $(\ell = e, \mu)$, and $b \to s\gamma\gamma$. In Section 5, we calculate the effects of the full set of $(\bar{s}b)(\bar{\tau}\tau)$ operators on Γ_{12}^s and analyze their numerical impact. Our model-independent findings are contrasted with two explicit SM extensions in Section 6. A summary of our main results and our conclusions are presented in Section 7. A series of appendices contains useful details concerning technical aspects of our calculations.

2 Preliminaries

In the SM, the effective $\Delta B = 1$ Lagrangian is given by

$$\mathcal{L}_{\text{eff}} = \mathcal{L}_{\text{QCD}\times\text{QED}}\,(u,d,s,c,b,e,\mu,\tau) + \frac{4G_F}{\sqrt{2}}\,V_{ts}^* V_{tb} \sum_i C_i(\mu) Q_i\,, \tag{19}$$

and consists of products of Wilson coefficients C_i and dimension-six operators Q_i. The Wilson coefficients C_i and the matrix elements of the operators Q_i both depend on the renormalization scale μ, which we set to the bottom-quark mass m_b throughout this article when evaluating the B-meson observables of interest. In (19) the Fermi constant G_F and the leading CKM factor $V_{ts}^* V_{tb}$ have been extracted as a global prefactor. Finally, the sum over i comprises the current-current operators ($i = 1, 2$), the QCD-penguin operators ($i = 3, 4, 5, 6$), the electromagnetic and chromomagnetic dipole operators ($i = 7, 8$), and the semileptonic operators ($i = 9, 10$).

For what concerns our work, the electromagnetic dipole and the vector-like semileptonic operator are the most important ones. We define them in the following way

$$Q_7 = \frac{e}{(4\pi)^2}\, m_b(\mu)\,(\bar{s}\,\sigma^{\mu\nu} P_R\, b)\, F_{\mu\nu}\,, \qquad Q_9 = \frac{e^2}{(4\pi)^2}\,(\bar{s}\,\gamma^\mu P_L\, b)\,\big(\bar{\ell}\,\gamma_\mu\,\ell\big)\,, \tag{20}$$

where e is the electromagnetic coupling constant, $m_b(\mu)$ denotes the $\overline{\text{MS}}$ bottom-quark mass, $F_{\mu\nu}$ is the field strength tensor associated to the photon, $P_{L,R} = (1 \mp \gamma_5)/2$ project onto left- and right-handed chiral fields, and $\sigma^{\mu\nu} = i\,[\gamma^\mu, \gamma^\nu]\,/2$. Within the SM one has numerically $C_{7,\text{SM}}(m_b) \approx -0.3$ and $C_{9,\text{SM}}(m_b) \approx 4.1$. The chiral-flipped partners Q_7' and Q_9' of the electromagnetic dipole and the vector-like semileptonic operator are obtained from (20) by simply replacing the chiral projectors $P_{L,R}$ through $P_{R,L}$.

In what follows, we supplement the effective SM Lagrangian (19) by

$$\mathcal{L}_{\text{eff}}^{\Lambda} = \frac{1}{\Lambda^2} \sum_i C_i^{\Lambda}(\mu) Q_i\,, \tag{21}$$

where $\Lambda > m_t$ denotes the scale of new physics and the index i runs over the complete set of dimension-six operators with flavor content $(\bar{s}b)(\bar{\tau}\tau)$, namely $(A, B = L, R)$

$$\begin{aligned} Q_{S,AB} &= (\bar{s}\,P_A\,b)\,(\bar{\tau}\,P_B\,\tau)\,, \\ Q_{V,AB} &= (\bar{s}\,\gamma^\mu P_A\,b)\,(\bar{\tau}\,\gamma_\mu P_B\,\tau)\,, \\ Q_{T,A} &= (\bar{s}\,\sigma^{\mu\nu} P_A\,b)\,(\bar{\tau}\,\sigma_{\mu\nu} P_A\,\tau)\,. \end{aligned} \tag{22}$$

As we will discuss in detail below, the Wilson coefficients of these operators can be bounded by various direct and indirect constraints for any given value of Λ.

For later convenience, we also introduce Wilson coefficients C_i associated to the non-standard operators (22) that are normalized like the SM contributions (19). In terms of the Wilson coefficients C_i^{Λ} they are simply given by

$$C_i(\mu) = \frac{\sqrt{2}}{4G_F}\,\frac{1}{V_{ts}^* V_{tb}}\,\frac{C_i^{\Lambda}(\mu)}{\Lambda^2}\,. \tag{23}$$

We now have enough definitions and notations in place to start the discussion of the relevant restrictions.

3 Direct Bounds on $(\bar{s}b)(\bar{\tau}\tau)$ Operators

The ten operators entering (21) govern the purely leptonic $B_s \to \tau^+\tau^-$ decay, the inclusive semi-leptonic $B \to X_s\tau^+\tau^-$ decay, and its exclusive counterpart $B^+ \to K^+\tau^+\tau^-$, making these channels potentially powerful constraints. In practice, however, flavor-changing neutral current $B_{d,s}$ decays into final states involving taus are experimentally still largely unexplored territory. Rather weak limits on the branching ratios of the former two modes can be derived from the LEP searches for B decays with large missing energy [37] and/or the B-factory measurements of the ratio of the B_s- and the B_d-meson lifetimes [23].

In the latter case, one finds by comparing the SM prediction $\tau_{B_s}/\tau_{B_d} - 1 \in [-0.4, 0.0]\%$ [3] with the corresponding experimental result $\tau_{B_s}/\tau_{B_d} - 1 = (0.4 \pm 1.9)\%$, which is based on the recent LHCb measurement $\Gamma_s = (0.656 \pm 0.012)\,\text{ps}^{-1}$ [14] and $\tau_{B_d} = (1.519 \pm 0.007)\,\text{ps}$ [38], good agreement compared to previous measurements [7]. Yet, following the arguments of [23], values of

$$\mathcal{B}(B_s \to \tau^+\tau^-) \,<\, 3\%\,, \tag{24}$$

are still allowed at 90% CL even after the first LHCb measurement.

Constraints also derive from the semileptonic branching ratios [9, 39]. For example, one can consider possible contaminations of the decay samples $b \to u\ell\bar{\nu}_\ell$ due to one tau in $B \to X_s\tau^+\tau^-$ decaying leptonically and the other one hadronically. If the second τ decays as $\tau^+ \to u(\bar{d},\,\bar{s})\,\bar{\nu}_\tau$ such a decay chain results in the experimental signature $B \to X_s\,\nu_\tau\bar{\nu}_\tau + (\pi^+, K^+)\,\ell\bar{\nu}_\ell$, which contains at least one strangeness final-state meson. Since this signal arises in the SM as a sequence of tree-level decays, one has very naively

$$\mathcal{B}(B \to X_s\tau^+\tau^-) \approx \frac{\mathcal{B}(B \to X_s\,\nu_\tau\bar{\nu}_\tau + (\pi^+, K^+)\,\ell\bar{\nu}_\ell)}{\mathcal{B}(\tau \to \ell\bar{\nu}_\ell\nu_\tau)\,\mathcal{B}(\tau^+ \to u(\bar{d},\,\bar{s})\,\bar{\nu}_\tau)}\,. \tag{25}$$

Using now [38]

$$\mathcal{B}(\tau \to \ell\bar{\nu}_\ell\nu_\tau) \approx 36\%\,, \qquad \mathcal{B}(\tau^+ \to u(\bar{d},\,\bar{s})\,\bar{\nu}_\tau) \approx 1 - \mathcal{B}(\tau \to \ell\bar{\nu}_\ell\nu_\tau) \approx 64\%\,, \tag{26}$$

and taking into account the uncertainties of the relevant semileptonic decay modes of $B^{0/\pm}$-admixture [38]

$$\begin{aligned}
\mathcal{B}(B \to K^+\,\ell\bar{\nu}_\ell + \text{anything}) &= (6.2 \pm 0.5)\cdot 10^{-2}\,,\\
\mathcal{B}(B \to K^-\,\ell\bar{\nu}_\ell + \text{anything}) &= (1.0 \pm 0.4)\cdot 10^{-2}\,,\\
\mathcal{B}(B \to K^0/\bar{K}^0\,\ell\bar{\nu}_\ell + \text{anything}) &= (4.6 \pm 0.5)\cdot 10^{-2}\,.
\end{aligned} \tag{27}$$

suggests that branching ratios satisfying

$$\mathcal{B}(B \to X_s\tau^+\tau^-) \,\lesssim\, 2.5\%\,, \tag{28}$$

would lead to no observable signal. Of course, a misidentification of $B \to X_s\,\nu_\tau\bar{\nu}_\tau + (\pi^+, K^+)\,\ell\bar{\nu}_\ell$ as an exclusive $B \to \pi\,\ell\bar{\nu}_\ell$ or an inclusive $B \to X_u\,\ell\bar{\nu}_\ell$ decay is also possible, *i.e.*, loosing the X_s in the analysis. In order to quantify the precise impact of misidentifications would obviously require a sophisticated analysis, including all the relevant details of the experimental analysis,

which goes beyond the scope of this work. Let us add that the above line of reasoning can also be applied to inclusive semileptonic B decays, if one knows the fraction $f_{\rm cut}$ of $B \to X_s\tau^+\tau^-$ events that survive the experimental cuts imposed in the $B \to X\ell\nu_\ell$ analysis. Employing $(\mathcal{B}_{\rm SL})_{\rm SM} = (11.7 \pm 1.4 \pm 1.0)\,\%$ [40, 41] and $(\mathcal{B}_{\rm SL})_{\rm exp} = (10.76 \pm 0.14)\,\%$ [38] leads to the limit

$$\mathcal{B}(B \to X_s\tau^+\tau^-) \lesssim \frac{21\%}{9.3 f_{\rm cut} - 1}\,. \tag{29}$$

The assumption $f_{\rm cut} = 1$, *i.e.*, that all $B \to X_s\tau^+\tau^-$ events represent a residual background, is quite unrealistic, but it yields the same numerical value as in (28). In practice $f_{\rm cut}$ can be determined only with a dedicated detector simulation, and hence we expect a significantly weaker constraint on $B \to X_s\tau^+\tau^-$ from $B \to X\ell\nu_\ell$. We finally note that $B \to X_s\tau^+\tau^-$ only starts to become competitive with the other direct constraints, if its branching ratios can be constrained to values below 1% (this will become clear only later). Whether (28) or the weaker limit of $\mathcal{O}(5\%)$ extracted in [37] is used, is hence irrelevant for (most of) the further discussion.

Bounds of strength similar to those given in (24) and (28) also follow from charm counting [42, 43]. Combining the latest BaBar result for the average of the B^- and B_d charm multiplicity $n_c = 1.20 \pm 0.06$ with $\mathcal{B}(B \to X_{sc\bar{c}}) = 0.24 \pm 0.02$ [44], yields $\mathcal{B}(B \to X_{\text{no charm}}) = (4 \pm 5)\%$ at 68% CL. Subtracting from this number the SM prediction for $\mathcal{B}(B \to X_{\text{no charm}})$ of around 1.5% [39], suggests that (24) is a conservative upper limit, that is consistent with charm counting.[8]

The unsatisfactory experimental situation concerning $B_{d,s}$-meson decays into final states with tau pairs, has been improved recently by the BaBar collaboration, which was able to set a first upper limit on the branching ratio of $B^+ \to K^+\tau^+\tau^-$. At 90% CL this bound is [46][9]

$$\mathcal{B}(B^+ \to K^+\tau^+\tau^-) < 3.3 \cdot 10^{-3}\,. \tag{30}$$

Although the limits (24) and (30) are many orders of magnitude above the corresponding SM predictions, we will see below that they provide currently the strongest constraints on the Wilson coefficients of the scalar and vector operators of $(\bar{s}b)(\bar{\tau}\tau)$ type. Let us first have a look at $B_s \to \tau^+\tau^-$ and $B \to X_s\tau^+\tau^-$. In the case of the exclusive decay the relevant branching ratio reads [47]

$$\mathcal{B}(B_s \to \tau^+\tau^-) = \mathcal{N}_{B_s\to\tau^+\tau^-} \left\{ \left(1 - \frac{4m_\tau^2}{M_{B_s}^2}\right) \left|F_S\right|^2 + \left|F_P + \frac{2m_\tau}{M_{B_s}}\, F_A\right|^2 \right\}, \tag{31}$$

where

$$\mathcal{N}_{B_s\to\tau^+\tau^-} = \frac{G_F^2 M_{B_s}^3 f_{B_s}^2 \tau_{B_s}}{16\pi} \left|V_{ts}^* V_{tb}\right|^2 \sqrt{1 - \frac{4m_\tau^2}{M_{B_s}^2}} \;\approx\; 6.4 \cdot 10^{-2}\,, \tag{32}$$

[8] The $B \to X_{\text{no charm}}$ branching ratio has also been determined by DELPHI [45]. The quoted 95% CL bound of $\mathcal{B}(B \to X_{\text{no charm}}) < 3.7\%$ relies however on a Monte Carlo simulation to model the displaced vertex distribution for intermediate charm, which introduces an uncertainty that is hard to quantify.

[9] The measurement is restricted to dilepton invariant masses of $14.23\ \text{GeV}^2 < q^2 < (M_{B^+} - M_{K^+})^2$. This experimental cut is implemented in our calculation.

$\lvert C_i(1\text{ TeV})\rvert$	$B_s \to \tau^+\tau^-$	$B \to X_s\tau^+\tau^-$	$B^+ \to K^+\tau^+\tau^-$
S, AB	0.3	1.9	0.5
V, AB	1.0	1.5	0.8
T, A	—	0.5	0.5

Table 1: Direct upper bounds on the high-scale Wilson coefficients at $\Lambda = 1$ TeV.

and

$$\begin{aligned} F_{S,P} &= \frac{M_{B_s}}{m_b + m_s}\Big[C_{S,RR} \mp C_{S,LL} \pm C_{S,RL} - C_{S,LR}\Big]\,, \\ F_A &= \frac{\alpha}{2\pi}\, C_{10,\text{SM}} + C_{V,LR} + C_{V,RL} - C_{V,LL} - C_{V,RR}\,. \end{aligned} \tag{33}$$

Here all Wilson coefficients are understood to be normalized as in (19) and (23) and evaluated at m_b. Notice also that the SM contribution proportional to $C_{10,\text{SM}}(m_b) \approx -4.2$ has been kept separately in F_A. Compared to the new-physics contribution this correction is suppressed by both a CKM and a loop factor, resulting in $\mathcal{B}(B_s \to \tau^+\tau^-)_{\text{SM}} \approx 8 \cdot 10^{-7}$. In order to obtain this number, we have employed $G_F = 1.16637 \cdot 10^{-5}\ \text{GeV}^{-2}$, $M_{B_s} = 5.3663$ GeV [38], $f_{B_s} = 238.8$ MeV [48], $\tau_{B_s} = 1.477$ ps [7], $|V_{ts}^* V_{tb}|^2 = 1.6 \cdot 10^{-3}$ [49], $m_\tau = 1.777$ GeV, and $\alpha = \alpha(M_Z) = 1/129$ [50].

Assuming the dominance of a single operator and neglecting the SM contribution to (33), we then find by combining (24) with (31) the following upper bounds on the magnitudes of the Wilson coefficients

$$|C_{S,AB}(m_b)| \,<\, 0.5\,, \qquad |C_{V,AB}(m_b)| \,<\, 1.0\,. \tag{34}$$

Here $m_b = m_b^{\text{pole}} = 4.8$ GeV and $m_s = 0.1$ GeV have been used.

By means of the solutions to the LO renormalization group equations (RGEs) presented in Appendix A, the results (34) can be reinterpreted as limits on the matching corrections to the Wilson coefficients at the scale Λ. Performing the evolution from m_b (m_t) up to m_t (Λ) in a five-flavor (six-flavor) theory, we obtain in the case of the scalar operators

$$|C_{S,AB}(\Lambda)| \,=\, \eta_5^{12/23}\,\eta_6^{4/7}\,|C_{S,AB}(m_b)| \,<\, \eta_6^{4/7}\,0.4\,, \tag{35}$$

where $\eta_5 = \alpha_s(m_t)/\alpha_s(m_b) \approx 0.5$ and $\eta_6 = \alpha_s(\Lambda)/\alpha_s(m_t) = [1.223 + 0.124 \ln(\Lambda/\text{TeV})]^{-1}$. The bound on $C_{V,AB}$ is, on the other hand, scale independent, because the vector operators $Q_{V,AB}$ correspond to conserved currents. In Table 1, we summarize for convenience the currently available direct bounds on the high-scale Wilson coefficients assuming a new-physics scale of $\Lambda = 1$ TeV.

Unlike $B_s \to \tau^+\tau^-$, the inclusive decay $B \to X_s\tau^+\tau^-$ depends on all Wilson coefficients. Its differential branching ratio might be split into the SM contribution, the interference of the SM with the new-physics contributions, and the pure new-physics corrections. Since we

assume that the Wilson coefficients of the operators (22) are generated at tree level, we are allowed to neglect both the SM and the interference terms, which are suppressed relative to the new-physics effects by at least a factor of order $\alpha/(4\pi) \approx 6 \cdot 10^{-4}$. The relevant contributions to the branching ratio differential in the dilepton invariant mass, $s = q^2$, read [51]

$$\left(\frac{d\mathcal{B}(B \to X_s\tau^+\tau^-)}{ds}\right)_i = \mathcal{N}_{B\to X_s\tau^+\tau^-}\, |C_i|^2\, M_i^{X_s}(s)\,. \tag{36}$$

Here $i = S, AB, V, AB, T, A$ and

$$\mathcal{N}_{B\to X_s\tau^+\tau^-} = \frac{3}{2m_b^8}\,\frac{|V_{ts}^* V_{tb}|^2}{|V_{cb}|^2}\,\frac{\mathcal{B}(B \to X_c\ell\nu_\ell)_{\rm exp}}{f(z)\,\kappa(z)} \;\approx\; 1.1\,\cdot 10^{-6}\,. \tag{37}$$

The analytic expressions for the kinematic functions $M_i^{X_s}(s)$ can be found in Appendix B. In order to obtain the numerical result in (37), we have employed $|V_{ts}^* V_{tb}|^2/|V_{cb}|^2 = 0.96$ [49], $\mathcal{B}(B \to X_c\ell\nu_\ell)_{\rm exp} = 10.23\%$ [7], and $z = (m_c^{\rm pole}/m_b^{\rm pole})^2 = 0.084$. For this input the phase-space factor and the NLO QCD corrections [52] of $B \to X_c\ell\nu_\ell$ evaluate to $f(z) \approx 0.54$ and $\kappa(z) \approx 0.88$. The Wilson coefficients are bounded by integrating the non-resonant branching ratio over the entire kinematical range $4m_\tau^2 < s < (m_b - m_s)^2$ and comparing the obtained result to the experimental extraction.[10] Numerically, the integrations yield

$$\int ds\, M_S^{X_s}(s) \approx 2636\,, \qquad \int ds\, M_V^{X_s}(s) \approx 10542\,, \qquad \int ds\, M_T^{X_s}(s) \approx 126505\,. \tag{38}$$

From the bound $\mathcal{B}(B \to X_s\tau^+\tau^-) \lesssim 2.5\%$, which is five orders of magnitude above the SM expectation $\mathcal{B}(B \to X_s\tau^+\tau^-)_{\rm SM} \approx 5 \cdot 10^{-7}$ [53], we then derive, by utilizing (36) to (38) and considering each type of Wilson coefficient individually, the inequalities

$$|C_{S,AB}(m_b)| \lesssim 2.9\,, \quad |C_{V,AB}(m_b)| \lesssim 1.5\,, \quad |C_{T,A}(m_b)| \lesssim 0.4\,. \tag{39}$$

Comparing these results with (34), one observes that $B \to X_s\tau^+\tau^-$ constrains the contributions arising from scalar and vector operators much less severely than $B_s \to \tau^+\tau^-$.

It is again straightforward to find the corresponding bounds on the high-scale Wilson coefficients. In the case of the scalar operators, one proceeds in analogy to (35), the upper bound on $C_{V,AB}$ is unchanged, and in the last case, we arrive at

$$|C_{T,A}(\Lambda)| \;=\; \eta_5^{-4/23}\,\eta_6^{-4/21}\,|C_{T,A}(m_b)| \;\lesssim\; \eta_6^{-4/21}\,0.5\,. \tag{40}$$

The bound (40) and the limits on $C_{S,AB}$ and $C_{V,AB}$ stemming from $B \to X_s\tau^+\tau^-$ are collected in Table 1.

Let us finally consider the bounds on the Wilson coefficients C_i that follow from the upper limit (30), which still leaves ample room for new physics to enhance the branching ratio with respect to the SM prediction of $\mathcal{B}(B^+ \to K^+\tau^+\tau^-)_{\rm SM} \approx 2 \cdot 10^{-7}$ [54]. Keeping again only the

[10] Experimentally the narrow ψ' resonance at $s \approx 13.7\,\text{GeV}^2$ has to be removed by making appropriate kinematic cuts in the invariant mass spectrum. In view of the poorness of the upper limit on $\mathcal{B}(B \to X_s\tau^+\tau^-)$, it is at present immaterial if these cuts are imposed in the theoretical calculation.

pure new-physics contributions, the individual corrections to the differential branching ratio of $B^+ \to K^+\tau^+\tau^-$ take the form [55]

$$\left(\frac{d\mathcal{B}(B^+ \to K^+\tau^+\tau^-)}{ds}\right)_i = \mathcal{N}_{B^+\to K^+\tau^+\tau^-}\,|C_i|^2\,M_i^{K^+}(s)\,, \tag{41}$$

where

$$\mathcal{N}_{B^+\to K^+\tau^+\tau^-} = \frac{G_F^2|V_{ts}^*V_{tb}|^2\tau_{B^+}}{24\pi^3 M_{B^+}^3} \;\approx\; 5.0\cdot 10^{-6}\,, \tag{42}$$

corresponding to $\tau_{B^+} = 1.641\,\text{ps}$ [7] and $M_{B^+} = 5.279\,\text{GeV}$ [38]. The functions $M_i^{K^+}(s)$ are collected in Appendix B. Integrating them over $14.23\,\text{GeV}^2 < s < (M_{B^+} - M_{K^+})^2$ gives

$$\int ds\, M_S^{K^+}(s) \approx 1081\,, \qquad \int ds\, M_V^{K^+}(s) \approx 1082\,, \qquad \int ds\, M_T^{K^+}(s) \approx 3610\,. \tag{43}$$

Inserting (42) and (43) into (41), and allowing for the presence of a single Wilson coefficient at a time, the upper bound (30) implies

$$|C_{S,AB}(m_b)| \,<\, 0.8\,, \qquad |C_{V,AB}(m_b)| \,<\, 0.8\,, \qquad |C_{T,A}(m_b)| \,<\, 0.4\,. \tag{44}$$

The limits on the Wilson coefficients at the scale $\Lambda = 1$ TeV following from $B^+ \to K^+\tau^+\tau^-$ are shown in Table 1. The quoted numbers have been obtained from (44) by simply applying the relations (35) and (40). We see that the exclusive $b \to s\tau^+\tau^-$ mode provides at present the most stringent direct constraints on the vector and tensor operators with flavor content $(\bar s b)(\bar\tau\tau)$, while it is less restrictive than $B_s \to \tau^+\tau^-$ for what concerns the scalar contributions. Notice also that the resummation of large leading logarithms of the form $\alpha_s^n \ln^n(\Lambda^2/m_b^2)$ makes the bound on $|C_{S,AB}(\Lambda)|$ ($|C_{T,AB}(\Lambda)|$) relative to the limit that applies to $|C_{S,AB}(m_b)|$ ($|C_{T,AB}(m_b)|$) stronger (weaker). The running effects are however moderate in both cases if new physics enters at the TeV scale, as they change the results by a factor of around 1.6 and 0.9 only. Numerically, we see that the direct constraints allow for effects that reach almost $\mathcal{O}(1)$ in all $|C_i(1\,\text{TeV})|$. Recalling that the dominant SM contribution to Γ_{12}^s arises from the color-singlet current-current operator $(\bar s\,\gamma^\mu P_L c)(\bar c\gamma_\mu P_L b)$, which has a Wilson coefficient of roughly 1 at the weak scale, we expect that the $(\bar s b)(\bar\tau\tau)$ operators can give a visible correction to the off-diagonal element of the decay matrix in the B_s-meson system. We however curb our enthusiasm and postpone a detailed numerical analysis of the new-physics effects in Γ_{12}^s to Section 5, to check first that the indirect constraints associated to operator mixing do not thwart these potentially large effects.

4 Indirect Bounds on $(\bar s b)(\bar\tau\tau)$ Operators

Further constraints on the Wilson coefficients (23) arise indirectly from the experimentally available information on the $b \to s\gamma$ and $b \to s\ell^+\ell^-$ ($\ell = e, \mu$) transitions, because some of the effective operators introduced in (22) mix into

$$Q_{7,A} = \frac{e}{g_s^2}\,m_\tau\,(\bar s\,\sigma^{\mu\nu}P_A\,b)F_{\mu\nu}\,, \qquad Q_{9,A} = \frac{e^2}{g_s^2}\,(\bar s\,\gamma^\mu P_A\,b)(\bar\ell\,\gamma_\mu\,\ell)\,, \tag{45}$$

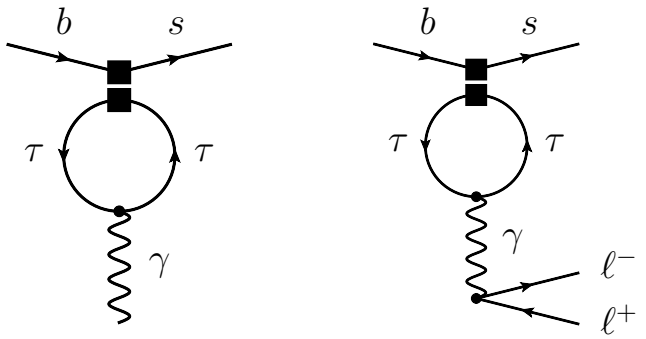


Figure 3: Diagrams with a penguin insertion of a $(\bar{s}b)(\bar{\tau}\tau)$ operator (black squares) that contribute to the renormalization and the matrix element of the electromagnetic dipole (left) and vector-like semileptonic (right) operators. The tau loop in both graphs is closed.

at the one-loop level. Here $A = L, R$. The corresponding Feynman diagrams are depicted in Figure 3. It is important to realize that due to the flavor structure of the $(\bar{s}b)(\bar{\tau}\tau)$ operators only insertions are possible in which the tau lines are joined and the photon is emitted from the resulting closed loop. Our results for the anomalous dimension matrix (ADM) describing the operator mixing of $Q_{S,AB}$, $Q_{V,AB}$, and $Q_{T,A}$ into $Q_{7,A}$ and $Q_{9,A}$ are given in Appendix A. We find that the ADM is sparse, because most of the relevant penguin diagrams either contain a vanishing Dirac trace or evaluate to zero due to current conservation. In particular, the operators $Q_{S,AB}$ mix neither into $Q_{7,A}$ nor $Q_{9,A}$,[11] while $Q_{V,AB}$ ($Q_{T,A}$) mixes only into $Q_{9,A}$ ($Q_{7,A}$). The possible one-loop mixing of the $(\bar{s}b)(\bar{\tau}\tau)$ operators is therefore much more restricted than what has been claimed in the articles [26, 30, 32], which all did not perform an explicit calculation of the one-loop ADM. We will see in a moment, that as a result of the particular mixing pattern, the stringent constraints from the radiative decay $B \to X_s\gamma$ rule out large contributions to Γ_{12}^s only if they arise from the tensor operators $Q_{T,A}$. Similarly, the rare decays $B \to X_s\ell^+\ell^-$ and $B \to K^{(*)}\ell^+\ell^-$ primarily limit contributions stemming from the vector operators $Q_{V,AB}$.

The new-physics corrections to the partonic $b \to s\gamma$ and $b \to s\ell^+\ell^-$ amplitudes involve the low-energy Wilson coefficients of the effective operators introduced in (45). Neglecting the matching corrections to both $Q_{7,A}$ and $Q_{9,A}$, *i.e.*, setting $C_{7,A}(\Lambda) = C_{9,A}(\Lambda) = 0$, we find from the analytic solutions to the RGEs as given in Appendix A, the following expressions

$$\begin{aligned} C_{7,A}(m_b) &= \eta_6^{4/21}\left(0.6 - \eta_6^{-1}\right) C_{T,A}(\Lambda)\,, \\ C_{9,A}(m_b) &= \left(0.1 - 0.2\,\eta_6^{-1}\right)\left(C_{V,AL}(\Lambda) + C_{V,AR}(\Lambda)\right). \end{aligned} \tag{46}$$

Determining the contributions of the operator sets (22) and (45) to the radiative and semileptonic $b \to s$ processes also requires the knowledge of the corresponding tree-level and

[11] Notice that scalar operators with flavor structure $(\bar{s}b)(\bar{q}q)$ with $q = s, b$ mix into the electromagnetic dipole and vector-like semileptonic operators at the one-loop level [56, 57]. The mixing arises from graphs constructed by joining two strange or bottom quarks belonging to the different disconnected parts of the composite operator and attaching the photon to the resulting open strange- or bottom-quark loop.

one-loop matrix elements. Details on these calculations are relegated to Appendix C. Following common practice, we include the effects of the relevant matrix elements by defining so-called effective Wilson coefficients [58]. For the SM operators Q_7 and Q_9 appearing in (20), we obtain at the scale $\mu = m_b$ the following new-physics corrections

$$\begin{aligned}\Delta C_7^{\rm eff}(s,m_b) &= \sqrt{x_\tau}\,\big(C_{7,R}(m_b) + M_7(\hat{s},x_\tau)\,C_{T,R}(m_b)\big)\,,\\ \Delta C_9^{\rm eff}(s,m_b) &= C_{9,L}(m_b) + M_9(\hat{s},x_\tau)\,\big(C_{V,LL}(m_b) + C_{V,LR}(m_b)\big)\,,\end{aligned} \tag{47}$$

with $C_{7,A}(m_b)$ and $C_{9,A}(m_b)$ given in (46) and $C_{T,A}(m_b) = 0.9\,\eta_6^{4/21}\,C_{T,A}(\Lambda)$. Furthermore, $\hat{s} = q^2/m_b^2$ and $x_\tau = m_\tau^2/m_b^2$. The analytic expressions for the functions $M_7(\hat{s},x_\tau)$ and $M_9(\hat{s},x_\tau)$ can be found in Appendix C. Analogous formulas hold in the case of the Wilson coefficients $\Delta C_7'^{\rm eff}(s,m_b)$ and $\Delta C_9'^{\rm eff}(s,m_b)$ of the chiral-flipped operators Q_7' and Q_9' after replacing $C_{i,R}(m_b)$ through $C_{i,L}(m_b)$ $\big(C_{i,LA}(m_b)$ through $C_{i,RA}(m_b)\big)$ in the first (second) line of (47). Notice that only $\Delta C_7^{\rm eff}(m_b) = \Delta C_7^{\rm eff}(0,m_b)$ and $\Delta C_7'^{\rm eff}(m_b) = \Delta C_7'^{\rm eff}(0,m_b)$ enter the prediction for $B\to X_s\gamma$, while all $\Delta C_i^{\rm eff}(s,m_b)$ and their chirality-flipped partners affect the $b\to s\ell^+\ell^-$ transitions.

In order to derive a bound on the Wilson coefficients $C_{T,A}$ at the high scale, we compare the experimental measurement of the $B\to X_s\gamma$ branching ratio with its SM prediction. For a photon-energy cut of $E_\gamma > 1.6$ GeV, the experimental world average reads [11]

$$\mathcal{B}(B\to X_s\gamma)_{\rm exp} = (3.55 \pm 0.24 \pm 0.09)\cdot 10^{-4}\,, \tag{48}$$

while the SM expectation is given by [59, 60][12]

$$\mathcal{B}(B\to X_s\gamma)_{\rm SM} = (3.15 \pm 0.23)\cdot 10^{-4}\,. \tag{49}$$

The good agreement between (48) and (49) puts stringent limits on the corrections $\Delta C_7^{\rm eff}(m_b)$ and $\Delta C_7'^{\rm eff}(m_b)$. Further non-negligible constraints on the magnitudes and phases of the corrections to the low-energy Wilson coefficients of the electromagnetic dipole operators arise from the inclusive [68] and exclusive [69] $b\to s\ell^+\ell^-$ transitions as well as the time-dependent CP-asymmetries and the isospin asymmetry in $B\to K^*\gamma$ [70]. Including all these constraints and allowing for the variation of a single effective Wilson coefficient at a time, we obtain the following 90% CL upper bounds

$$|\Delta C_7^{\rm eff}(m_b)| \,<\, 0.23\,, \qquad |\Delta C_7'^{\rm eff}(m_b)| \,<\, 0.20\,. \tag{50}$$

Notice that since we are treating the Wilson coefficients as complex, the upper limit on the magnitude of $\Delta C_7^{\rm eff}(m_b)$ is weaker by almost a factor of 6 than the bound that holds in the case of a real coefficient. In contrast, the bound on $|\Delta C_7'^{\rm eff}(m_b)|$ is not affected by whether the correction is treated as complex or real, because Q_7' does not interfere with the SM contribution to first order. We also remark that the $B\to K^{(*)}\ell^+\ell^-$ observables are more efficient than

[12] Several NNLO QCD corrections (see [61, 62, 63, 64, 65, 66] and partly [67]) that were calculated after the publication of [59, 60] are not included in the central value of the SM prediction, but remain within the perturbative higher-order uncertainty of 3% that has been estimated in the latter two articles.

$B \to K^*\gamma$ in restricting the allowed values of the real and especially the imaginary parts of $\Delta C_7^{\rm eff}(m_b)$.

Utilizing (46) and (47), the limits (50) translate into

$$|C_{T,R}(\Lambda)| \,=\, \eta_6^{17/21}\,(0.4+2.3\,\eta_6)^{-1}\,|\Delta C_7^{\rm eff}(m_b)| \,<\, \eta_6^{-4/21}\left(10.2+1.8\,\eta_6^{-1}\right)^{-1}\,, \qquad (51)$$

and an analog inequality, obtained by replacing $|\Delta C_7^{\rm eff}(m_b)|$, 10.2, and 1.8 by $|\Delta C_7^{\prime\rm eff}(m_b)|$, 11.8, and 2.1, holds in the case of $C_{T,L}$. For a new-physics scale of $\Lambda = 1$ TeV the numerical values of the bounds on $|C_{T,A}(\Lambda)|$ are given in Table 2. Notice that as a result of the resummation of large logarithms the bounds on the low-scale Wilson coefficients of the tensor operators are a factor of around 1.2 stronger than those on the initial conditions.

The magnitudes of the Wilson coefficients $C_{V,AB}$ can be bounded by comparing the available data on the inclusive [71, 72, 73, 74] and exclusive [75, 76, 77, 78, 80, 79, 81] $b \to s\ell^+\ell^-$ transitions with the corresponding theoretical predictions that include the corrections $\Delta C_9^{\rm eff}(s,m_b)$ and $\Delta C_9^{\prime\rm eff}(s,m_b)$. Our global analysis of rare semileptonic B decays relies on the article [50] for what concerns $B \to X_s\ell^+\ell^-$ and on the works [69, 82, 83, 84, 85] in the case of $B \to K^{(*)}\ell^+\ell^-$. The used data[13] includes the branching ratios $\mathcal{B}(B \to X_s\ell^+\ell^-)$ and $\mathcal{B}(B \to K^{(*)}\ell^+\ell^-)$, the forward-backward asymmetry $A_{\rm FB}(B \to K^*\ell^+\ell^-)$, as well as the longitudinal K^* polarization fraction $F_L(B \to K^*\ell^+\ell^-)$. In all cases, we consider the low-s region of dilepton invariant masses $s = [1,6]$ GeV^2. At high s we consider for $B \to X_s\ell^+\ell^-$ the region $s > 14.4$ GeV^2 and for $B \to K^{(*)}\ell^+\ell^-$ the two bins $s = [14.18, 16]$ GeV^2 and $s > 16$ GeV^2. At 90% CL our global analysis returns the following upper bounds

$$|\Delta C_9^{\rm eff}(s,m_b)| \,<\, 2.0\,, \qquad |\Delta C_9^{\prime\rm eff}(s,m_b)| \,<\, 1.7\,, \qquad (52)$$

when the corrections to the effective Wilson coefficients are treated as additive, s-independent contributions and only a single correction is allowed to float at a time.

The inequalities (52) can be converted into bounds on the magnitudes of the high-scale values of $C_{V,AB}$ using (46) and (47). Since the expressions for $\Delta C_9^{\rm eff}(s,m_b)$ and $\Delta C_9^{\prime\rm eff}(s,m_b)$ depend explicitly on s through the function $M_9(\hat{s},m_\tau)$, we extract the limits directly from our global fit. We find the following exclusion

$$|C_{V,LA}(\Lambda)| \,=\, \left(2.0-0.2\,\eta_6^{-1}\right)^{-1}\,|\Delta C_9^{\rm eff}(s,m_b)| \,<\, 2.0\left(2.0-0.2\,\eta_6^{-1}\right)^{-1}\,. \qquad (53)$$

An analog formula holds for $|C_{V,RA}(\Lambda)|$ after replacing $|\Delta C_9^{\rm eff}(s,m_b)|$ and the factor 2.0 in front of the bracket by $|\Delta C_9^{\prime\rm eff}(s,m_b)|$ and 1.7. Assuming a new-physics scale of $\Lambda = 1$ TeV, one finds the numerical values given Table 2.

In contrast to $B \to X_s\gamma$, all $(\bar{s}b)(\bar{\tau}\tau)$ operators contribute to the double-radiative $B_{d,s}$-meson decays at the one-loop level [86, 87]. In the following, we will concentrate on the case

[13] Our fit is based on [71, 72], [77, 79, 80, 81], and [77, 79] for what concerns $B \to X_s\ell^+\ell^-$, $B \to K^*\ell^+\ell^-$, and $B \to K\ell^+\ell^-$, respectively. The latest (but still preliminary) Belle measurement of $\mathcal{B}(B \to X_s\ell^+\ell^-)$ [73], which finds a low-s branching ratio of around 2.4σ below the SM prediction, is not used, because the quoted central values of the branching fractions for electrons and muons in the final state differ by a factor of more than 2. If only the LHCb measurements of $B \to K^*\ell^+\ell^-$ [80] are used, the numbers in (50), (52), and Table 2 read 0.29 and 0.20, 3.1 and 2.5, and 1.5, 1.2, 0.07, and 0.13, respectively. While some of these bounds are not as strong as the limits based on the combined $B \to K^{(*)}\ell^+\ell^-$ data [77, 79, 80, 81], they clearly show the large impact (and future potential) of LHCb measurements on the extraction of low-energy Wilson coefficients.

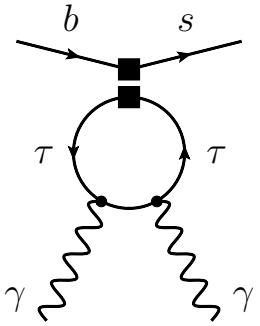


Figure 4: 1PI diagram with a penguin insertion of a $(\bar{s}b)(\bar{\tau}\tau)$ operator (black squares) that contribute to the $b \to s\gamma\gamma$ amplitude. The tau loop in the graph is closed and the diagram with interchanged photons is not shown.

of $B_s \to \gamma\gamma$, which turns out to give the strongest constraints on the Wilson coefficients of the operators under consideration. At the quark level the double-radiative $b \to s\gamma\gamma$ decays receive contributions from one-particle irreducible (1PI) diagrams of the type shown in Figure 4 as well as similar one-particle reducible (1PR) graphs in which at least one of the two photons is radiated from an external leg. Since the 1PR diagrams are proportional to the tree-level matrix elements of $Q_7^{(\prime)}$, their contributions are included if the corresponding amplitudes are expressed through the effective Wilson coefficients $C_7^{(\prime)\text{eff}}$. A detailed discussion of the calculation of the one-loop matrix elements can be found in Appendix D.

Experimentally so far only upper limits on the branching ratio of $B_s \to \gamma\gamma$ exist. At 90% CL the most stringent limit is [88]

$$\mathcal{B}(B_s \to \gamma\gamma)_{\text{exp}} < 8.7 \cdot 10^{-6} \,. \tag{54}$$

In order to constrain the Wilson coefficients of the $(\bar{s}b)(\bar{\tau}\tau)$ operators also a value for the branching ratio of $B_s \to \gamma\gamma$ within the SM is needed. Updating the analysis of [89, 90], we obtain

$$\mathcal{B}(B_s \to \gamma\gamma)_{\text{SM}} = \left(0.7^{+2.5}_{-0.4}\right) \cdot 10^{-6} \,, \tag{55}$$

where the dominant part of the quoted error is due to the hadronic parameter λ_B, which parametrizes the first negative moment of the B-meson wave function. Estimates of λ_B are very uncertain, but typically fall in the range between 0.25 GeV and 0.75 GeV [91, 92, 93, 94], and the central value in (55) corresponds to $\lambda_B = 0.5$ GeV. Numerically subleading errors in the latter SM prediction arise from the variation of the renormalization scale and the error on the decay constant f_{B_s}.

Assuming the dominance of a single operator, we then find by combining (54) and (55) the following 90% CL upper bounds on the magnitudes of the Wilson coefficients $(A, B = L, R)$

$$\begin{aligned} |\Delta C_7^{\text{eff}}(m_b)| < 2.2 \,, \quad |\Delta C_7^{\prime\text{eff}}(m_b)| < 1.9 \,, \\ |C_{S,AL}(m_b)| < 3.4 \,, \quad |C_{S,AR}(m_b)| < 2.3 \,, \quad |C_{V,AB}(m_b)| < 5.9 \,. \end{aligned} \tag{56}$$

Clearly, these limits are not competitive with the bounds obtained earlier from the other tree- and loop-level mediated $B_{d,s}$-meson decays. The reason for the weakness of these bounds is

$\lvert C_i(1\text{ TeV})\rvert$	$b \to s\gamma, s\ell^+\ell^-, s\gamma\gamma$
S, AB	—
V, LA	1.1
V, RA	1.0
T, L	0.07
T, R	0.08

Table 2: Indirect upper bounds on the high-scale Wilson coefficients at $\Lambda = 1$ TeV.

threefold. First, as shown in Appendix D, the 1PI contributions of the $(\bar{s}b)(\bar{\tau}\tau)$ operators are power suppressed, second, the experimental bound (54) leaves room for order of magnitude enhancements of $\mathcal{B}(B_s \to \gamma\gamma)$ with respect to the SM expectation, and third the theoretical errors plaguing (55) are large. Notice that the power suppression of four-fermion operator contributions is a generic feature of the $B_s \to \gamma\gamma$ decay in the heavy-quark limit [89, 90], which is absent in the case of $B \to K\gamma\gamma$ [87]. The sensitivity of the latter decay mode to $(\bar{s}b)(\bar{\tau}\tau)$ operators is therefore in principle more pronounced than the one of $B_s \to \gamma\gamma$. In practice, however, the possibility to extract short-distance information from $B \to K\gamma\gamma$ is severely limited. First, the perturbative part of the $B \to K\gamma\gamma$ spectrum is not accessible behind the large resonance peaks associated to $B \to K\eta_c \to K\gamma\gamma$ *etc.* and, second, not even an upper limit on $\mathcal{B}(B \to K\gamma\gamma)$ is currently available. Hence the bounds (56) represent at present the most stringent limits on the low-energy Wilson coefficients of interest that can be derived from double-radiative $B_{d,s}$-meson decays.

With a large amount of luminosity collected at a super-flavor factory it might also be possible to measure the CP asymmetry [95]

$$r_{\rm CP} = \frac{|\mathcal{A}(\bar{B}_s \to \gamma\gamma)|^2 - |\mathcal{A}(B_s \to \gamma\gamma)|^2}{|\mathcal{A}(\bar{B}_s \to \gamma\gamma)|^2 + |\mathcal{A}(B_s \to \gamma\gamma)|^2}\,, \tag{57}$$

besides the $B_s \to \gamma\gamma$ branching ratio. The SM prediction of $r_{\rm CP}$ reads

$$(r_{\rm CP})_{\rm SM} = (0.5^{+0.6}_{-0.3})\%\,. \tag{58}$$

The largest fraction in the quoted error is due to the scale dependence, followed by the uncertainty coming from λ_B. The smallness of (58) implies that finding $r_{\rm CP}$ at or above the 10% level would constitute an unambiguous signal of the presence of additional sources of direct CP violation. In fact, the complex Wilson coefficients of the $(\bar{s}b)(\bar{\tau}\tau)$ operators give rise to such an effect and thus allow to change $r_{\rm CP}$ dramatically. Employing the 90% CL bounds on the low-energy Wilson coefficients of $|C_{S,AB}(m_b)| < 0.5$, $|C_{V,AB}(m_b)| < 0.8$, $|\Delta C_7^{\rm eff}(m_b)| < 0.29$, and $|\Delta C_7^{\prime\rm eff}(m_b)| < 0.19$, we find that the CP asymmetry in $B_s \to \gamma\gamma$ can vary in the ranges $(r_{\rm CP})_{S,AL} \in [-95, 95]\%$, $(r_{\rm CP})_{S,AR} \in [-40, 40]\%$, $(r_{\rm CP})_{V,AB} \in [-70, 70]\%$, $(r_{\rm CP})_{T,L} \in [-20, 20]\%$, and $(r_{\rm CP})_{T,R} \in [-70, 70]\%$, for the respective Wilson coefficient with an arbitrary phase. In order to measure $r_{\rm CP}$, SuperB (Belle II) probably needs to collect at least $75\,{\rm ab}^{-1}$

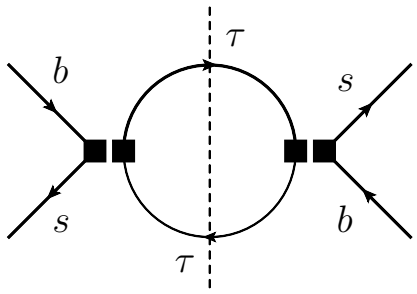


Figure 5: Diagram with a double insertion of a $(\bar{s}b)(\bar{\tau}\tau)$ operator (black squares) that contributes to Γ_{12}^s at LO. The tau loop in the diagram is closed and the cut (dashed line) indicates that only the imaginary part of the graph furnishes a correction to the off-diagonal element of the decay-width matrix.

$(50\,\text{ab}^{-1})$ of data, a goal that is expected to be achieved in the year 2021. This implies that the $B_s \to \gamma\gamma$ decay will not be able to provide useful additional information on the possible size of $(\bar{s}b)(\bar{\tau}\tau)$ contributions in the near future.

By comparing the results displayed in Table 1 with those shown in Table 2, one observes that the bounds on the high-scale Wilson coefficients $C_i(\Lambda)$ that stem from the direct constraints, *i.e.*, the rare decays $B_s \to \tau^+\tau^-$, $B \to X_s\tau^+\tau^-$, and $B^+ \to K^+\tau^+\tau^-$, are currently in 8 out of 10 cases stronger than those that follow from the indirect constraints, *i.e.*, the $b \to s\gamma$, $b \to s\ell^+\ell^-$, and $b \to s\gamma\gamma$ transitions. The only exception are the Wilson coefficients $C_{T,A}(\Lambda)$ of the tensor operators, which are tightly bound as a result of the one-loop mixing of $Q_{T,A}$ into the electromagnetic dipole operators Q_7 and Q_7', which give the dominant contribution to the $B \to X_s\gamma$ rate. On the other hand, sizable effects in $C_{S,AB}(\Lambda)$ and $C_{V,AB}(\Lambda)$, that can almost compete with the leading current-current SM interactions in strength, are allowed, because rare B_s and B_d decays involving a tau pair in the final state are so poorly constrained. While the direct constraints are unlikely to change notable with almost all BaBar and Belle data analyzed, the indirect bounds on the vector operators are expected to improve with LHCb precision measurements of $B \to K^{(*)}\ell^+\ell^-$ under way.

5 Effects of $(\bar{s}b)(\bar{\tau}\tau)$ Operators in Γ_{12}^s

The off-diagonal element of the decay-width matrix is related via the optical theorem to the absorptive part of the forward-scattering amplitude which converts a $\bar{B}_s$ into a B_s meson. Working to LO in the strong coupling constant and Λ_{QCD}/m_b, the contributions from the complete set of operators (22) to Γ_{12}^s is found by computing the matrix elements between quark states depicted in Figure 5. Details on the actual calculation are given in Appendix E. Considering again only the self-interference of a single $(\bar{s}b)(\bar{\tau}\tau)$ operator at a time, we obtain

in terms of the hadronic matrix elements $\langle Q_i\rangle = \langle B_s|Q_i|\bar{B}_s\rangle$ of the following $\Delta B = 2$ operators

$$\begin{aligned} Q_S^A &= (\bar{s}\, P_A\, b)\, (\bar{s}\, P_A\, b)\ , \\ \tilde{Q}_S^A &= (\bar{s}_\alpha\, P_A\, b_\beta)\, (\bar{s}_\beta\, P_A\, b_\alpha)\ , \\ Q_V^A &= (\bar{s}\, \gamma^\mu P_A\, b)\, (\bar{s}\, \gamma_\mu P_A\, b)\ , \end{aligned} \tag{59}$$

the results

$$\begin{aligned} (\Gamma_{12}^s)_{S,LA} &= \mathcal{N}_{\Gamma_{12}^s}\, 3\, x_\tau \beta_\tau \left\langle Q_S^L\right\rangle (C_{S,LA})^2\,, \\ (\Gamma_{12}^s)_{V,LA} &= \mathcal{N}_{\Gamma_{12}^s}\, \beta_\tau \left[(1-x_\tau)\left\langle Q_V^L\right\rangle + (1+2x_\tau)\left\langle Q_S^R\right\rangle\right] (C_{V,LA})^2\,, \\ (\Gamma_{12}^s)_{T,L} &= -\mathcal{N}_{\Gamma_{12}^s}\, 12\, x_\tau \beta_\tau \left[4\left\langle Q_S^L\right\rangle + 8\left\langle \tilde{Q}_S^L\right\rangle\right] (C_{T,L})^2\,. \end{aligned} \tag{60}$$

Here α, β are color indices and we have introduced $\beta_\tau = \sqrt{1-4x_\tau}$ as well as

$$\mathcal{N}_{\Gamma_{12}^s} = -\frac{G_F^2 m_b^2}{6\pi M_{B_s}} (V_{ts}^* V_{tb})^2\,. \tag{61}$$

The corresponding expressions for $(\Gamma_{12}^s)_{S,RA}$, $(\Gamma_{12}^s)_{V,RA}$, and $(\Gamma_{12}^s)_{T,R}$ are obtained from (60) by exchanging the labels L and R everywhere. Following common practice, we express the matrix elements in terms of hadronic parameters B_i. In our analysis, we employ

$$\left\langle Q_S^A\right\rangle = -\frac{5}{12}\, f_{B_s}^2 M_{B_s}^2 B_S\,, \qquad \left\langle \tilde{Q}_S^A\right\rangle = \frac{1}{12}\, f_{B_s}^2 M_{B_s}^2 \tilde{B}_S\,, \qquad \left\langle Q_V^A\right\rangle = \frac{2}{3}\, f_{B_s}^2 M_{B_s}^2 B_V\,, \tag{62}$$

with $f_{B_s} = 231\,\text{MeV}$ [9], $B_S \approx 1.3$, $\tilde{B}_S \approx 1.4$ [96], $B_V \approx 0.84$ [9], and the meson states normalized as $\langle B_s|B_s\rangle = \langle \bar{B}_s|\bar{B}_s\rangle = 2M_{B_s}$. Notice that the latter value of f_{B_s} has been used to obtain the SM predictions $(\Delta\Gamma_s)_{\text{SM}}$ and $(a_{fs}^s)_{\text{SM}}$ presented in (4) and (7), respectively.

The direct and indirect constraints discussed in Sections 3 and 4 restrict the magnitude of the low-energy Wilson coefficients but not their relative weak phase. We can thus determine only the maximal[14] allowed value of the parameter R_Γ introduced in (14) in a model-independent fashion. Allowing the new-physics contribution of one operator at a time to be non-zero, the corresponding inequality is given in terms of the off-diagonal elements of the decay matrix (60) by

$$(R_\Gamma)_i < 1 + \frac{2\,|(\Gamma_{12}^s)_i|}{(\Delta\Gamma_s)_{\text{SM}}}\, \cos(\phi_{J/\psi\phi}^s)_{\text{SM}} \approx 1 + \frac{2\,|(\Gamma_{12}^s)_i|}{(\Delta\Gamma_s)_{\text{SM}}}\,. \tag{63}$$

Numerically, we find for the individual contributions

$$\begin{aligned} (R_\Gamma)_{S,AB} &< 1 + (0.4 \pm 0.1)\, |C_{S,AB}(m_b)|^2\,, \\ (R_\Gamma)_{V,AB} &< 1 + (0.4 \pm 0.1)\, |C_{V,AB}(m_b)|^2\,, \\ (R_\Gamma)_{T,A} &< 1 + (3.6 \pm 0.9)\, |C_{T,A}(m_b)|^2\,, \end{aligned} \tag{64}$$

[14] Of course, there is also a model-independent lower limit on $(R_\Gamma)_i$. It corresponds to full destructive interference and is obtained from (63) and (64) by replacing the plus with minus signs.

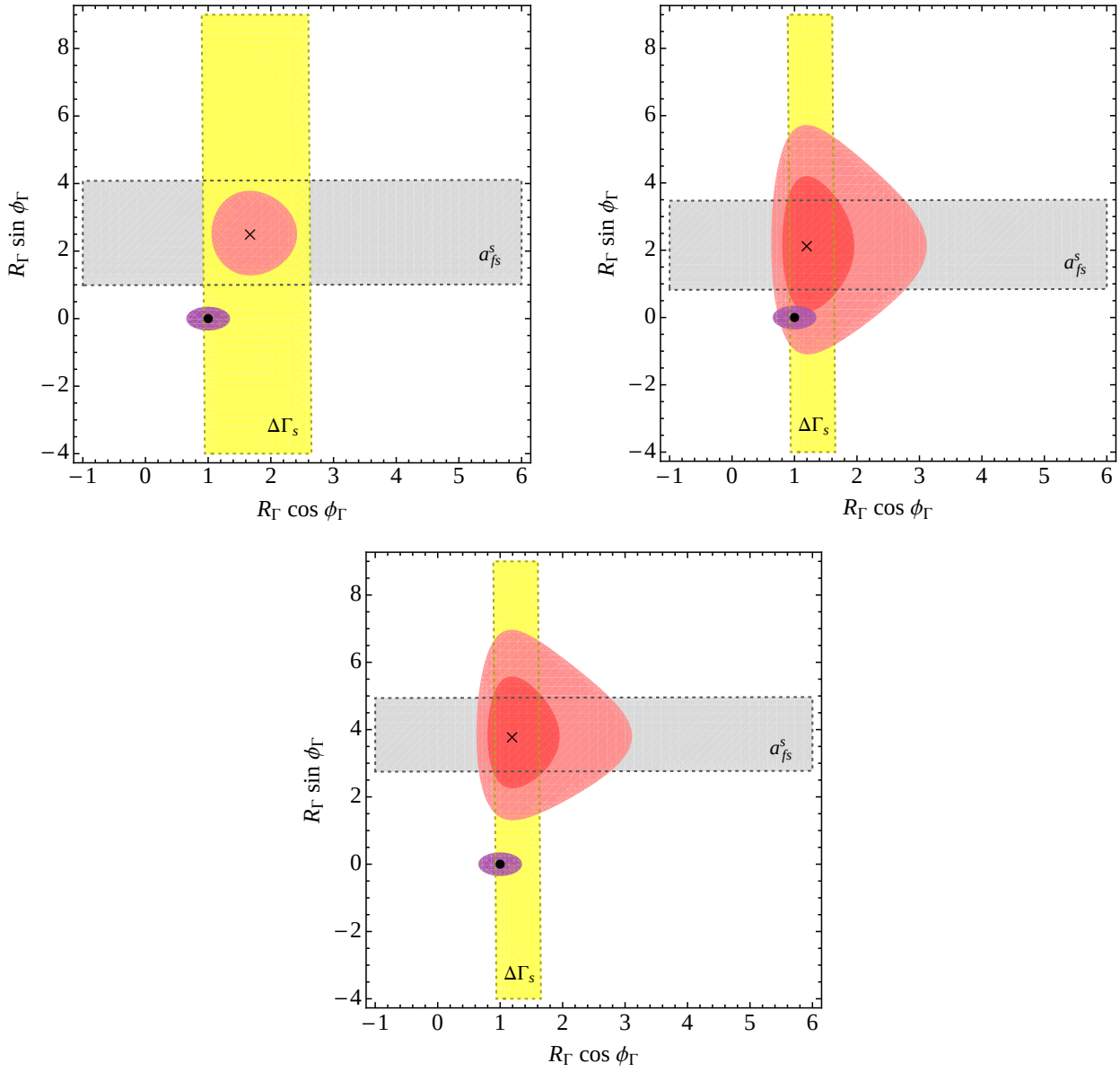


Figure 6: Upper left (upper right, lower): Constraints from $\Delta\Gamma_s$ and a^s_{fs} on the parameter R_Γ and ϕ_Γ in scenario S2 employing the data set D1 (D2, D3). The yellow and gray bands represent 68% CL regions (dofs = 1), while the purple ellipses illustrate the parameter space that is accessible for $|C_{V,AB}(m_b)| < 0.8$ and $C_{S,AB}(m_b) = C_{T,A}(m_b) = 0$. For comparison, the 68% (95%) probability region of the combined fit to the B_s-meson mixing data (dofs = 2) is shown in red (light red). In all panels the SM prediction (best-fit solution) is indicated by a dot (cross).

where the quoted uncertainties are due to the error on $(\Delta\Gamma_s)_{\rm SM}$ as given in (4). Employing now the 90% CL bounds on the low-energy Wilson coefficients derived in the previous two sections, *i.e.*, $|C_{S,AB}(m_b)| < 0.5$, $|C_{V,AB}(m_b)| < 0.8$, $|C_{T,L}(m_b)| < 0.06$, and $|C_{T,R}(m_b)| < 0.09$,

it follows that

$$(R_\Gamma)_{S,AB} < 1.15\,, \qquad (R_\Gamma)_{V,AB} < 1.35\,, \qquad (R_\Gamma)_{T,L} < 1.02\,, \qquad (R_\Gamma)_{T,R} < 1.04\,. \tag{65}$$

These numbers imply that $(\bar{s}b)(\bar{\tau}\tau)$ operators of scalar (vector) type can lead to enhancements of $|\Gamma_{12}^s|$ over its SM value by 15% (35%) without violating any existing constraint. In contrast, contributions from tensor operators can alter $|\Gamma_{12}^s|$ by at most 4%, because larger corrections would be at variance with $B \to X_s\gamma$.

In Figure 6 we compare the parameter space in the $R_\Gamma \cos\phi_\Gamma$–$R_\Gamma \sin\phi_\Gamma$ plane that can be populated in scenario S2 with $|C_{V,AB}(m_b)| < 0.8$ and $C_{S,AB}(m_b) = C_{T,A}(m_b) = 0$ (purple ellipses) to the constraints imposed by the measurement of $\Delta\Gamma_s$ and a_{fs}^s (yellow and gray bands). The upper left and right panel correspond to the data set D1 and D2, respectively, while the lower panel illustrates the situation in the case of the D3 data set. We see that the contribution of a single vector operator with flavor structure $(\bar{s}b)(\bar{\tau}\tau)$ can lead to an improvement of the fit. For example, in the case of the new data set D2 an agreement with the data at 68% CL (red area) can be achieved. It is however also evident that the best-fit solution (cross) of both data sets cannot be accommodated. The allowed parameter space is further reduced for scalar and tensor operators, so that we do not explicitly display these cases in the figures. This demonstrates that absorptive new physics in Γ_{12}^s in form of $(\bar{s}b)(\bar{\tau}\tau)$ operators cannot provide a satisfactory explanation of the anomaly in the dimuon charge asymmetry data observed by the DØ collaboration.

6 New-Physics Models

So far our discussion has been completely general since we parametrized the new-physics effects in terms of effective couplings of higher-dimensional operators. We now will consider explicit scenarios of new physics that can give rise to $(\bar{s}b)(\bar{\tau}\tau)$ operators with large Wilson coefficients. Discussions similar to ours have been presented previously in [23, 29, 30, 35], where it was found that new-physics models containing leptoquarks or Z' boson may explain the observed tensions in the B_s-meson data. In the following we will show that this is not the case. Our work hence clarifies and extends these existing studies.

We first consider scenarios with leptoquarks (LQ), *i.e.*, color-triplet or -antitriplet particles carrying both lepton (L) and baryon (B) number. Such new degrees of freedom are encountered in various extensions of the SM, such as grand unified theories, technicolor, and composite models (see [97, 98, 99, 100] for topical reviews). At low energies, the interactions between the SM particles and the LQs can be captured by writing down the most general Lagrangian compatible with renormalizability, L and B conservation, and invariance under the SM gauge group. These general requirements allow for scalar and vector LQs interacting directly with the SM fermions as well as for LQ couplings to the Higgs boson.

In the following, we will elaborate in detail only on the case of $SU(2)$ singlet scalar LQs. From our discussion it should however become clear how the given results have to be adapted to cover the other cases. The relevant interaction terms involving a charged lepton, a down-type quark, and a $SU(2)$ singlet scalar LQ are given by

$$\mathcal{L}_{\rm LQ} \supset (\lambda_{R\tilde{S}_0})_{ij}\, \bar{d}_j^c P_R\, e_i\, \tilde{S}_0 + \text{h.c.}\,. \tag{66}$$

Here $\lambda_{R\tilde{S}_0}$ is a complex 3×3 matrix in the lepton and quark flavor spaces, d_i and e_i are $SU(2)$ SM singlets, and the subscript of $\tilde{S}_0$ indicates the $SU(2)$ transformation property of the LQ. After integrating out the LQ and performing a Fierz rearrangement, the interactions (66) give rise to a $\Delta B = 1$ $(\bar{s}b)(\bar{\tau}\tau)$ operator of vector type. Explicitly, one finds

$$\mathcal{L}_{\text{eff}} \supset -\frac{(\lambda^*_{R\tilde{S}_0})_{32}(\lambda_{R\tilde{S}_0})_{33}}{2M^2_{\tilde{S}_0}}\, Q_{V,RR}\,, \tag{67}$$

where $M_{\tilde{S}_0}$ denotes the mass of $\tilde{S}_0$. The coefficient multiplying the operator $Q_{V,RR}$ is bound by the requirement $|C_{V,AB}(\mu)| < 0.8$, which holds for any scale μ. Numerically, we find

$$\frac{|(\lambda^*_{R\tilde{S}_0})_{32}(\lambda_{R\tilde{S}_0})_{33}|}{M^2_{\tilde{S}_0}} < 2.1\,\text{TeV}^{-2}\,. \tag{68}$$

The same bound also applies to the possible $SU(2)$ doublet scalar LQs (commonly denoted by S_2 and $\tilde{S}_2$ in the literature), which generate $Q_{V,LR}$ operators, after an appropriate replacement of couplings and masses.

Importantly, the interactions (66) give rise to corrections to both Γ^s_{12} and M^s_{12}. The contribution to the former quantity arise from a double insertion of (67). Applying the general formulas (60) to the specific case of a scalar LQ, we obtain

$$(\Gamma^s_{12})_{\text{LQ}} = -\frac{1}{288\pi}\,\frac{\left((\lambda^*_{R\tilde{S}_0})_{32}(\lambda_{R\tilde{S}_0})_{33}\right)^2}{M^4_{\tilde{S}_0}}\,\beta_\tau\left[(1-x_\tau)B_V - \frac{5}{8}(1+2x_\tau)B_S\right] m_b^2 f_{B_s}^2 M_{B_s}\,. \tag{69}$$

This formula disagrees with the analytic expression first given in [35], which does not contain terms proportional to B_S at all. Numerically, the difference amounts to a factor of around -0.4, with our result being smaller in magnitude. The correction to M^s_{12} originates from the box diagram displayed on the left-hand side of Figure 7. In agreement with [35], we find for this contribution[15]

$$(M^s_{12})_{\text{LQ}} = \frac{1}{384\pi^2}\,\frac{\left((\lambda^*_{R\tilde{S}_0})_{32}(\lambda_{R\tilde{S}_0})_{33}\right)^2}{M^2_{\tilde{S}_0}}\,\hat{\eta}_{B_s} I(a_\tau) f_{B_s}^2 M_{B_s} B_V\,, \tag{70}$$

where $\hat{\eta}_{B_s} = \eta_5^{6/23} \approx 0.8$ encodes the QCD corrections due to RG running and the Inami-Lim function $I(a)$ reads

$$I(a) = \frac{1+a}{(1-a)^2} + \frac{2a}{(1-a)^3}\,\ln a\,. \tag{71}$$

Notice that the above function approaches 1 for $a \to 0$, which is the relevant limit, since $a_\tau = m_\tau^2/M^2_{\tilde{S}_0} \ll 1$ for LQ masses at or above the electroweak scale.

Combining now (69) and (70), one obtains numerically

$$r_{\text{LQ}} = \frac{(M^s_{12})_{\text{LQ}}}{(\Gamma^s_{12})_{\text{LQ}}} = 2084\left(\frac{M_{\tilde{S}_0}}{250\text{ GeV}}\right)^2 = 2084\, z_{\tilde{S}_0}\,, \tag{72}$$

[15] We integrate out the top quark and the LQ simultaneously and consequently neglect small RG effects in the six-flavor theory.

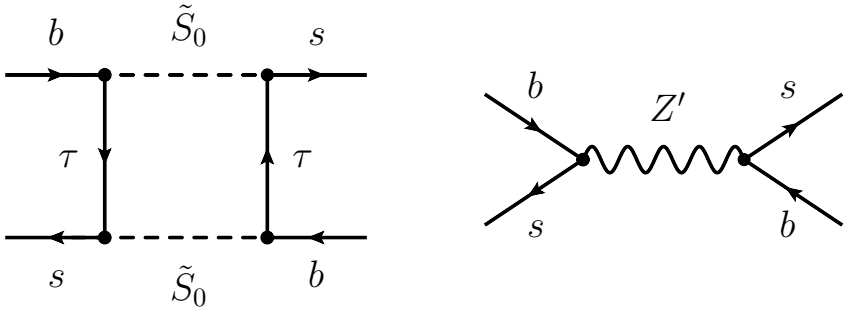


Figure 7: Left: One-loop contribution to M_{12}^s arising from a box diagram involving tau leptons and $SU(2)$ singlet scalar LQs. Right: Tree-level contribution to M_{12}^s associated to the exchange of a Z' boson.

which is real and positive. In contrast, $r_{\rm SM} = (M_{12}^s)_{\rm SM}/(\Gamma_{12}^s)_{\rm SM} \approx -200\exp\left(i\phi_{\rm SM}^s\right) \approx -200$. Notice also that (72) scales as $M_{\tilde{S}_0}^2$ which reflects the fact that $(M_{12}^s)_{\rm LQ}$ arises from a dimension-six correction (single operator insertion), whereas $(\Gamma_{12}^s)_{\rm LQ}$ stems from a dimension-eight contribution (operator double insertion).

In fact, given that ΔM_s (or equivalently R_M) is bounded experimentally, the sign and magnitude of $r_{\rm LQ}$ completely determine the ranges of possible R_Γ, $\Delta\Gamma_s$, and a_{fs}^s values in the LQ scenario (66). In Appendix F we show that this is a feature of all new-physics scenarios with real $(M_{12}^s)_{\rm NP}/(\Gamma_{12}^s)_{\rm NP}$. Applying the general formula (F4) to the case at hand, we find at 90% CL

$$0.96 = 1 - \frac{0.03}{z_{\tilde{S}_0}} < (R_\Gamma)_{\rm LQ} < 1 + \frac{0.2}{z_{\tilde{S}_0}} = 1.31\,. \tag{73}$$

Here the bound on R_M given in (16) and (17) has been used and the final numerical values have been obtained for $M_{\tilde{S}_0} = 210$ GeV, which represents the current 95% CL lower bound on third-generation scalar LQs decaying to a $b\tau$ final state [101]. Comparing (73) to the relevant model-independent upper bound, *i.e.*, the inequality in (65) involving $(R_\Gamma)_{V,AB}$, we see that at present both limits are (accidentally) almost the same. Since the bound on $M_{\tilde{S}_0}$ will improve with the LHC collecting more and more luminosity as we speak, the model-dependent upper limit will, however, soon become stronger than the model-independent one.

Similarly, one finds from the general formulas (F5) and (F6), the following two double inequalities

$$\begin{aligned} -0.11\ {\rm ps}^{-1} &= -\left(1 + \frac{0.2}{z_{\tilde{S}_0}}\right)(\Delta\Gamma_s)_{\rm SM} < (\Delta\Gamma_s)_{\rm LQ} < \left(1 + \frac{0.02}{z_{\tilde{S}_0}}\right)(\Delta\Gamma_s)_{\rm SM} = 0.09\,{\rm ps}^{-1}\,, \\ -0.7\cdot 10^{-2} &= -331\left(1 + \frac{0.1}{z_{\tilde{S}_0}}\right)(a_{fs}^s)_{\rm SM} < (a_{fs}^s)_{\rm LQ} < 331\left(1 + \frac{0.1}{z_{\tilde{S}_0}}\right)(a_{fs}^s)_{\rm SM} = 0.7\cdot 10^{-2}\,. \end{aligned} \tag{74}$$

These numbers imply that light singlet scalar LQs can change the predictions for $\Delta\Gamma_s$ and a_{fs}^s with respect to the SM expectations (4) and (7) by a factor of more than -1.3 and ± 375, respectively. In contrast, a strong enhancement of $\Delta\Gamma_s$ is not possible.[16] The maximal

[16] In [33] significant violations of $\Delta\Gamma_s \le (\Delta\Gamma_s)_{\rm SM}$ were reported. We are unable to reproduce this finding.

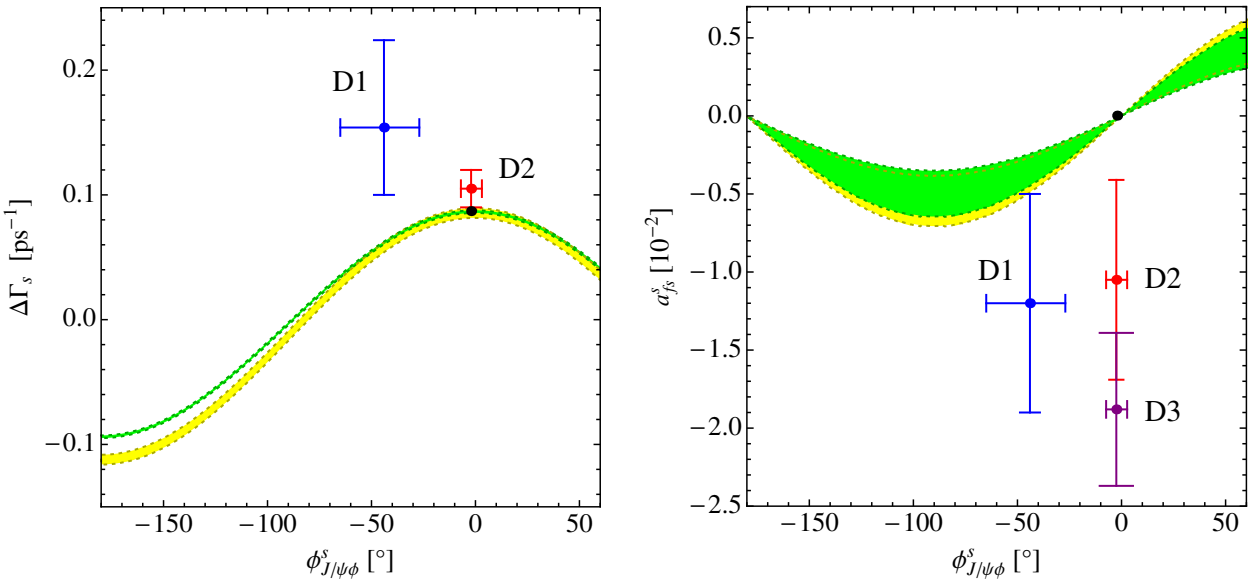


Figure 8: Predictions for $\Delta\Gamma_s$ (left) and a^s_{fs} (right) as a function of $\phi^s_{J/\psi\phi}$ in the presence of a singlet scalar LQ with $M_{\tilde{S}_0} = 210$ GeV (yellow areas) and $M_{\tilde{S}_0} = 400$ GeV (green areas). Since the left (right) panel is symmetric (antisymmetric) under $\phi^s_{J/\psi\phi} \leftrightarrow -\phi^s_{J/\psi\phi}$ only positive values of $\phi^s_{J/\psi\phi}$ up to 50° are shown. In both panels, the blue (red) error bar corresponds to the data set D1 (D2), while the SM point is indicated as a black point. The purple error bar in the right panel indicates the D3 data set. See text for details.

effects do, however, not occur simultaneously, since the observables in question are strongly correlated, as can be seen from Figure 8. In both panels the parameter space that is accessible at 90% CL, assuming a singlet scalar LQ mass of 210 GeV (400 GeV), is indicated in yellow (green). We see that $\Delta\Gamma_s$ becomes maximal (minimal) for $\phi^s_{J/\psi\phi} = 0°$ ($\phi^s_{J/\psi\phi} = -180°$) and that the LQ predictions form a band with a cosine-like shape (left panel). The predictions for a^s_{fs}, on the other hand, are minimal for $\phi^s_{J/\psi\phi} = 0°, -180°$ and maximal for $\phi^s_{J/\psi\phi} = -90°$, and the borders of the accessible parameter space in the $\phi^s_{J/\psi\phi}$–a^s_{fs} plane are sine curves (right panel). Notice that the cosine- and sine-like behavior of the predictions is an immediate consequence of (15). By comparing the accessible parameter space to the experimentally preferred regions, we see from the yellow colored regions that at 68% CL none of the considered data sets, *i.e.*, D1 (blue error bars), D2 (red error bars), and D3 (purple error bar), can be accommodated by a light singlet scalar LQ. Increasing the LQ mass, reduces the allowed parameter space, as can be seen from the green areas, further limiting the possible improvement of the tension in the B_s-meson sector.[17]

[17]While this work was being completed, the preprint [102] appeared, which performs a dedicated global fit of scalar LQ couplings, utilizing an assortment of tree- and loop-level observables in the charged lepton and quark sector. This article finds that the tension in the B_s-meson system cannot be cured by LQs, if one wants to explain the anomaly of the anomalous magnetic moment of the muon, $(g-2)_\mu$, and simultaneously fulfill the bounds on lepton-flavor violating processes. Notice, however, that if the former requirement is dropped,

The above general considerations are readily applied to the case of vector-like LQs. Considering for example LQ interactions of the form $\mathcal{L}_{\rm LQ} \supset (\lambda_{RV_0})_{ij}\, \bar{d}_j \gamma_\mu P_R\, e_i\, V_0^\mu + \text{h.c.}$ will lead to an effective Lagrangian $\mathcal{L}_{\rm eff} \supset -(\lambda^*_{RV_0})_{32}(\lambda_{RV_0})_{33}/M_{V_0}^2\, Q_{V,RR}$ with M_{V_0} denoting the mass of the vector-like LQ. It follows that the model-independent bound on such a LQ is twice as strong as the limit derived in (68). Furthermore, the ratio between $(M_{12}^s)_{\rm LQ}$ and $(\Gamma_{12}^s)_{\rm LQ}$ is found to be equal to the result given in (72). This tells us that (for $M_{V_0} = M_{\tilde{S}_0}$) the possible effects in $\Delta\Gamma_s$ and a_{fs}^s due to V_0 are identical to those originating from $\tilde{S}_0$. Vector-like LQs thus fail to reproduce the data sets D1 and D2 at 68% CL as well. Notice finally, that the situation is utterly hopeless, if one considers LQ couplings to the Higgs boson, since after a Fierz rearrangement the corresponding effective scalar interactions with flavor structure $(\bar{s}\tau)(\bar{\tau}b)$ contain tensor operators, which are most tightly constrained by the model-independent bounds (65).

We now switch gear and consider SM extensions where the gauge group contains an additional $U(1)'$ factor and the resulting Z' boson possess family non-universal, flavor-changing couplings [103]. Such new degrees of freedom arise in many well-motivated new-physics models, such as grand unified theories and/or string constructions (see [38, 104] for comprehensive reviews). In the physical basis, the flavor-changing neutral currents generically appear at tree level in both the left- and right-handed sectors. The interaction Lagrangian relevant for the further discussion can be written as

$$\mathcal{L}_{Z'} \supset \frac{g}{\cos\theta_W}\left[\left(\kappa_{sb}^L\, \bar{s}\,\gamma^\mu P_L\, b + \kappa_{sb}^R\, \bar{s}\,\gamma^\mu P_R\, b + \text{h.c.}\right) + \kappa_{\tau\tau}^L\, \bar{\tau}\,\gamma^\mu P_L\, \tau + \kappa_{\tau\tau}^R\, \bar{\tau}\,\gamma^\mu P_R\, \tau\right] Z'_\mu\,, \quad (75)$$

where g is the $SU(2)$ coupling of the SM and $\cos\theta_W$ denotes the cosine of the weak mixing angle. The Z'-boson coupling constant does not appear explicitly in (75), because it has been absorbed into the $\kappa_{ij}^{L,R}$ factors. Notice that the flavor off-diagonal couplings are in general complex, while the diagonal ones have to be real due to the hermiticity of the Lagrangian. Integrating out the Z' boson leads to the following $\Delta B = 1$ four-fermion interactions

$$\mathcal{L}_{\rm eff} \supset -\frac{8G_F}{\sqrt{2}}\,\frac{M_Z^2}{M_{Z'}^2}\,\kappa_{sb}^A\,\kappa_{\tau\tau}^B\, Q_{V,AB}\,. \quad (76)$$

Here $M_{Z'}$ denotes the mass of the extra $U(1)'$ gauge boson. From the numbers collected in Table 1, it follows that

$$\frac{|\kappa_{sb}^A\,\kappa_{\tau\tau}^B|}{M_{Z'}^2} < 1.9\,\text{TeV}^{-2}\,. \quad (77)$$

After integrating out the Z' boson, the interactions (75) give rise to one-loop corrections to Γ_{12}^s as well as tree-level corrections to M_{12}^s. In the following, we restrict ourselves to the case of purely left-handed interactions. The inclusion of right-handed currents is however straightforward. For Γ_{12}^s, we find in accordance with [29]

$$(\Gamma_{12}^s)_{Z'} = -\frac{4G_F^2}{9\pi}\left(\frac{M_Z^2}{M_{Z'}^2}\right)^2 \left(\kappa_{sb}^L\kappa_{\tau\tau}^L\right)^2 \beta_\tau\left[(1-x_\tau)B_V - \frac{5}{8}(1+2x_\tau)B_S\right] m_b^2 f_{B_s}^2 M_{B_s}\,. \quad (78)$$

no bound on $|(\lambda^*_{R\tilde{S}_0})_{32}(\lambda_{R\tilde{S}_0})_{33}|/M^2_{\tilde{S}_0}$ can be derived from the rare decays considered in the latter paper.

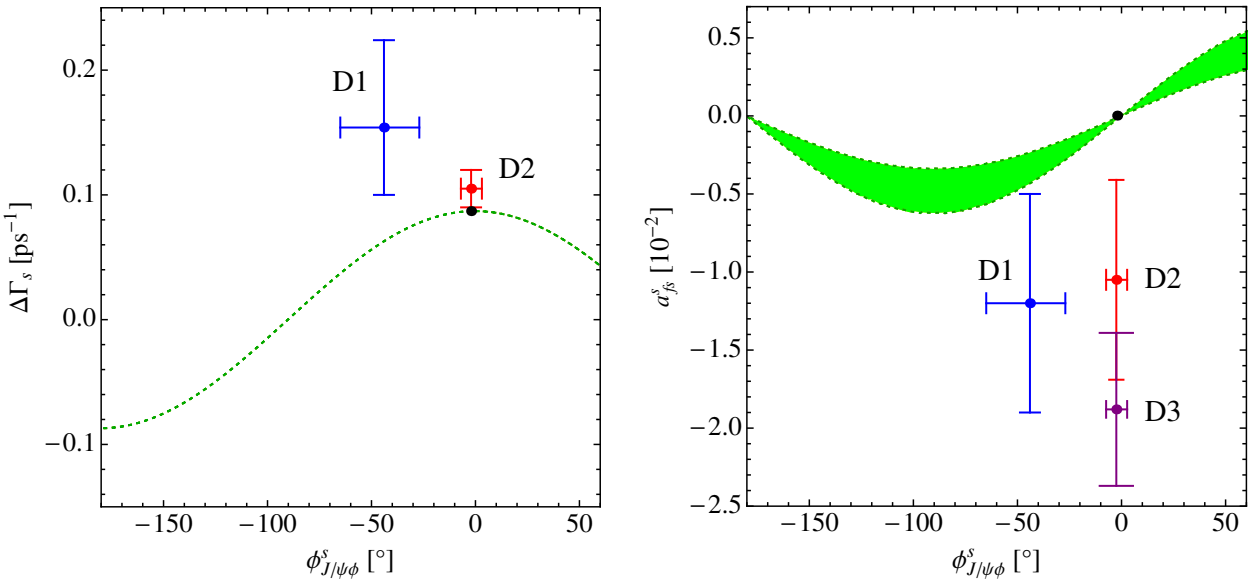


Figure 9: Predictions for $\Delta\Gamma_s$ (left) and a^s_{fs} (right) as a function of $\phi^s_{J/\psi\phi}$ in the presence of a Z' with $M_{Z'} = 400$ GeV (yellow areas) and $M_{Z'} = 1000$ GeV (green areas), which both overlap completely. Since the left (right) panel is symmetric (antisymmetric) under $\phi^s_{J/\psi\phi} \leftrightarrow -\phi^s_{J/\psi\phi}$ only positive values of $\phi^s_{J/\psi\phi}$ up to 50° are shown. In both panels, the blue (red) error bar corresponds to the data set D1 (D2), while the SM point is indicated as a black point. The purple error bar in the right panel indicates the D3 data set. See text for details.

The element M^s_{12} receives contributions from the graph shown on the right-hand side of Figure 7. A simple tree-level calculation leads to [105]

$$(M^s_{12})_{Z'} = \frac{4G_F}{3\sqrt{2}}\,\frac{M_Z^2}{M_{Z'}^2}\,\left(\kappa^L_{sb}\right)^2\,\hat\eta_{B_s} f_{B_s}^2 M_{B_s} B_V\,. \tag{79}$$

The ratio of (79) and (78) is given in semi-numerical form by

$$r_{Z'} = 6.0\cdot 10^5\,\left(\frac{M_{Z'}}{250\text{ GeV}}\,\frac{1}{\kappa^L_{\tau\tau}}\right)^2 = 6.0\cdot 10^5\,y_{Z'}\,. \tag{80}$$

It is real and positive. Notice that the numerical coefficient in (80) is enhanced relative to (72) by a loop factor and thus very large. From the discussion in Appendix F it hence follows that the effects of a Z' boson in R_Γ, $\Delta\Gamma_s$, and a^s_{fs} are severely constrained. Explicitly, we find

$$\begin{aligned} 1 - \frac{1.0\cdot 10^{-4}}{y_{Z'}} < (R_\Gamma)_{Z'} < 1 + \frac{7.7\cdot 10^{-4}}{y_{Z'}}\,, \\ -\left(1 + \frac{7.7\cdot 10^{-4}}{y_{Z'}}\right)(\Delta\Gamma_s)_{\rm SM} < (\Delta\Gamma_s)_{Z'} < \left(1 + \frac{7.0\cdot 10^{-5}}{y_{Z'}}\right)(\Delta\Gamma_s)_{\rm SM}\,, \end{aligned} \tag{81}$$

$$-331\left(1+\frac{3.3\cdot 10^{-4}}{y_{Z'}}\right)(a_{fs}^s)_{\rm SM} < (a_{fs}^s)_{Z'} < 331\left(1+\frac{3.3\cdot 10^{-4}}{y_{Z'}}\right)(a_{fs}^s)_{\rm SM}\,.$$

The Z'-boson mass $M_{Z'}$ is constrained by direct searches for resonant production of tau lepton pairs. At present the best bound is provided by the CDF measurement [106], which rules out a Z' with SM-like couplings to $q\bar{q}$ and $\tau^+\tau^-$ and a mass below 399 GeV at 95% CL. Although this bound is model-dependent,[18] we will use it as a guideline and consider a relatively light Z'-boson of $M_{Z'} = 400\,\text{GeV}$ as well as a heavier one with $M_{Z'} = 1000\,\text{GeV}$. The Z'-boson predictions in the $\phi_{J/\psi\phi}^s$–$\Delta\Gamma_s$ ($\phi_{J/\psi\phi}^s$–a_{fs}^s) plane are shown in the left (right) panel of Figure 9. The parameter space of 90% probability is depicted in yellow (green) for $M_{Z'} = 400$ GeV ($M_{Z'} = 1000$ GeV), which both overlap completely. While the shapes of the colored areas resemble the ones of Figure 8, one observes that compared to the case of LQs the allowed parameter space is even more reduced for a $U(1)'$ gauge boson. In particular, a Z' boson with mass at or above the electroweak scale and purely left-handed perturbative couplings clearly fails to describe the B_s-meson data within 68% CL. Because the parameter $r_{Z'}$ as defined in (80) is of the order $G_F^{-1} m_b^{-2} M_{Z'}^2/M_Z^2$ and therefore generically large, the latter statement is also true if the Z' boson couples only right-handed or both left- and right-handed.

7 Summary

Motivated by the observation that the anomalously large dimuon charge asymmetry measured by the DØ collaboration, can be fully explained only if new physics contributes to the absorptive part of the B_s–$\bar{B}_s$ mixing amplitude, we have presented a model-independent study of the contributions to Γ_{12}^s arising from the complete set of dimension-six operators with flavor content $(\bar{s}b)(\bar{\tau}\tau)$. Taking into account the direct bounds from $B_s \to \tau^+\tau^-$, $B \to X_s\tau^+\tau^-$, and $B^+ \to K^+\tau^+\tau^-$ as well as the indirect constraints from $b \to s\gamma$, $b \to s\ell^+\ell^-$ ($\ell = e, \mu$), and $b \to s\gamma\gamma$, we have demonstrated that only the Wilson coefficients of the tensor operators are severely constrained by data, while those of the scalar and vector operators can be sizable and almost reach the size of the Wilson coefficient of the leading current-current operator in the standard model. The model-independent 90% CL limits on the magnitudes of the Wilson coefficients are summarized in Table 3. Given these loose bounds, it follows that the presence of a single $(\bar{s}b)(\bar{\tau}\tau)$ operator can lead to an enhancement of Γ_{12}^s of at most 35% compared to its standard model value. Since a resolution of the tension in the B_s-meson sector would require the effects to be of the order of 300% (or larger), the allowed shifts are by far too small to provide a satisfactory explanation of the issue. We emphasize that after minor modifications, our general results can be applied to other dimension-six operators involving quarks and leptons. For example, as a result of the 90% CL limit $\mathcal{B}(B^+ \to K^+\tau^\pm\mu^\mp) < 7.7\cdot 10^{-5}$ [109], the direct bounds on the Wilson coefficients of the set of $(\bar{s}b)(\bar{\tau}\mu)$ operators turn out to be roughly a factor of 7 stronger than those in the $(\bar{s}b)(\bar{\tau}\tau)$ case. Possible effects of $(\bar{s}b)(\bar{\tau}\mu)$ operators are therefore generically too small to lead to a notable improvement of the tension present in the

[18] The mass $M_{Z'}$ and the couplings $\kappa_{\tau\tau}^{L,R}$ are constrained by the LEP measurement of the Z-boson couplings to taus [107]. Applying the results of the one-loop $Z \to f\bar{f}$ form factors given in [108], we find that even for couplings close to the non-perturbative limit the resulting bound is however with $M_{Z'} \gtrsim 25$ GeV rather weak. We will not entertain the possibility of a very light Z'-boson in the following.

Operator	Bound on Λ ($C_i^\Lambda = 1$)	Bound on C_i^Λ ($\Lambda = 1$ TeV)	Observable
$(\bar{s}\,P_A\,b)(\bar{\tau}\,P_B\,\tau)$	2.0 TeV	$4.2 \cdot 10^{-1}$	$B_s \to \tau^+\tau^-$
$(\bar{s}\,\gamma^\mu P_A\,b)(\bar{\tau}\,\gamma_\mu P_B\,\tau)$	1.0 TeV	1.1	$B^+ \to K^+\tau^+\tau^-$
$(\bar{s}\,\sigma^{\mu\nu} P_L\,b)(\bar{\tau}\,\sigma_{\mu\nu} P_L\,\tau)$	3.2 TeV	$9.2 \cdot 10^{-2}$	$B \to X_s\gamma$
$(\bar{s}\,\sigma^{\mu\nu} P_R\,b)(\bar{\tau}\,\sigma_{\mu\nu} P_R\,\tau)$	2.8 TeV	$1.1 \cdot 10^{-1}$	$B \to X_s\gamma$

Table 3: Model-independent limits on the Wilson coefficients of all possible four-fermion operators with flavor structure $(\bar{s}b)(\bar{\tau}\tau)$. The second column shows the bound on the suppression scale Λ assuming an effective coupling strength of $C_i^\Lambda = 1$, while the third column gives the value for C_i^Λ for a new-physics scale of $\Lambda = 1$ TeV. Notice that only the bounds on the tensor operators depend on the specific chirality $A, B = L, R$.

current $B_{d,s}$-meson data. Similarly, a contribution from $(\bar{d}b)(\bar{\tau}\tau)$ operators to Γ_{12}^d large enough to explain the $A_{\rm SL}^b$ data is excluded by the 90% CL bound $\mathcal{B}(B \to \tau^+\tau^-) < 4.1 \cdot 10^{-3}$ [110]. Naively, also $(\bar{b}d)(\bar{c}c)$ operators are heavily constrained (meaning that their Wilson coefficients should be smaller than those of the QCD/electroweak penguins in the standard model) by the plethora of exclusive B decays. A dedicated analysis of the latter class of contributions is however not available in the literature.

Our model-independent study of non-standard effects in Γ_{12}^s is complemented by an analysis of B_s–$\bar{B}_s$ mixing in two explicit standard model extensions. We consider in detail the corrections to M_{12}^s and Γ_{12}^s due to a $SU(2)$ singlet scalar leptoquark and a left-handed Z' boson with a mass at or above the electroweak scale. In both cases, we find that depletions of order one in $\Delta\Gamma_s$ and changes by more than two orders of magnitude in a_{fs}^s can occur, while a notable enhancement of the former quantity with respect to its standard model value is not possible. The large effects do, however, not occur simultaneously, since the non-standard contributions to M_{12}^s and Γ_{12}^s are strongly correlated in the considered new-physics scenarios. While $\Delta\Gamma_s$ becomes maximal (minimal) for $\phi_{J/\psi\phi}^s = 0°$ ($\phi_{J/\psi\phi}^s = -180°$) and the predictions form a band with a cosine-like shape in the $\phi_{J/\psi\phi}^s$–$\Delta\Gamma_s$ plane, a_{fs}^s is minimal for $\phi_{J/\psi\phi}^s = 0°, -180°$ and maximal for $\phi_{J/\psi\phi}^s = -90°$, and the accessible parameter space in the $\phi_{J/\psi\phi}^s$–a_{fs}^s plane is bounded by sine curves. In turn, neither a $SU(2)$ singlet scalar leptoquark nor a left-handed Z' boson renders a significant better description of the current data than the standard model. The same conclusion also applies to vector-like leptoquarks and Z' bosons with right-handed or both left- and right-handed couplings. In fact, we have shown that the pattern of deviations found in the case of leptoquarks and Z' bosons is a feature of all new-physics model with real $(M_{12}^s)_{\rm NP}/(\Gamma_{12}^s)_{\rm NP}$ and that in this class of models the measurement of ΔM_s generically puts stringent constraints on both $\Delta\Gamma_s$ and a_{fs}^s. As it turns out, these bounds are weakest if the ratio $r_{\rm NP} = (M_{12}^s)_{\rm NP}/(\Gamma_{12}^s)_{\rm NP}$ is positive and as small as possible. Since on dimensional grounds $r_{\rm NP}$ scales as the square of the new-physics scale, this general observation implies that standard model extensions that aim at a good description of the Tevatron data should have new degrees of freedom below the electroweak scale and/or be equipped with a mechanism that renders the contribution to M_{12}^s small. Furthermore, models in which $(M_{12}^s)_{\rm NP}$ is gener-

ated beyond Born level seem more promising, since in such a case $r_{\rm NP}$ is suppressed by a loop factor with respect to the case where $(M_{12}^s)_{\rm NP}$ arises already at tree level.

The above discussion implies that a full explanation of the observed discrepancies is not even possible for the most general case $(M_{12}^s)_{\rm NP} \neq 0$ and $(\Gamma_{12}^s)_{\rm NP} \neq 0$. Numerically, we find that the addition of a single $(\bar{s}b)(\bar{\tau}\tau)$ vector operator giving $(R_\Gamma)_{V,AB} = 1.35$ on top of dispersive new physics with $(M_{12}^s)_{\rm NP} \neq 0$, can only improve the quality of the fit to the latest set of measurements (*i.e.*, (1), (5), and (13)) to $\chi^2 = 1.2$ compared to $\chi^2 = 3.2$ within the standard model. This might indicate that the high central value of $A_{\rm SL}^b$ observed by the DØ collaboration is (partly) due to a statistical fluctuation. Future improvements in the measurement of the CP phase $\phi_{J/\psi\phi}^s$ and, in particular, a first determination of the difference $a_{fs}^s - a_{fs}^d$ between the B_s and B_d semileptonic asymmetries by LHCb, are soon expected to shed light on this issue. Will these measurements continue to make a case for new physics in Γ_{12}^s? Time will tell!

Acknowledgments

We are grateful to Yossi Nir for his critical questions that allowed us to spot mistakes in (60), (64), (65), and (E7). A big "thank you" to Sacha Davidson, Florian Goertz, Alex Kagan, Jernej Kamenik, Alex Lenz, and Quim Matias for useful discussions concerning leptoquarks, B_s–$\bar{B}_s$ mixing, charm counting, and radiative and semileptonic $b \to s$ decays. We furthermore thank Gudrun Hiller for reminding us of the role of $(\bar{s}b)(\bar{\tau}\tau)$ operators in $b \to s\gamma\gamma$ transitions. We are also grateful to Kevin Flood and Malachi Schram for helpful informations about experimental aspects of $B^+ \to K^+\tau^+\tau^-$. Stimulating discussions with Christian Bauer and Bogdan Dobrescu in June 2010 at the Aspen Workshop "Forefront QCD and LHC Discoveries", which triggered the present research, are acknowledged. UH thanks finally the Aspen Center for Physics for hospitality and the NSF (Grant No. 1066293) for partial support.

A Operator Mixing

In the following we present the analytic expressions that are needed to evolve the Wilson coefficients from the high-energy scale Λ down to the low-energy scale m_b. In the basis $(Q_{S,AL}, Q_{V,AL}, Q_{T,A}, Q_{7,A}, Q_{9,A})$ with $A = L, R$ the LO ADM, which describes the mixing of these operators, reads

$$\gamma_s = \frac{\alpha_s}{4\pi} \begin{pmatrix} -8 & 0 & 0 & 0 & 0 \\ 0 & 0 & 0 & 0 & \frac{4}{3} \\ 0 & 0 & \frac{8}{3} & 8 & 0 \\ 0 & 0 & 0 & \frac{8}{3} - 2\beta_s & 0 \\ 0 & 0 & 0 & 0 & -2\beta_s \end{pmatrix}, \tag{A1}$$

where $\beta_s = 11 - 2/3 N_f$ and N_f denotes the number active quark flavors. Notice that the self-mixing of $Q_{S,AL}$ is, up to an overall sign, equal to the one of the quark mass. This has to be the case, because a composite operator built out of a scalar current and a quark mass is conserved and thus has zero anomalous dimension. Furthermore, the self-mixings of $Q_{T,A}$ and $Q_{7,A}$ are the same, up to the factor $-2\beta_s$ (which is due to the normalization of $Q_{7,A}$), since the tau mass does not run in QCD. Of course, the result (A1), which after a suitable replacement of color and charge factors agrees with [56, 57], also holds for the operators $(Q_{S,AR}, Q_{V,AR}, Q_{T,A}, Q_{7,A}, Q_{9,A})$ given that gluon interactions conserve chirality.

Solving the RGEs, we find that the Wilson coefficients at the scale $\mu_1 < \mu_0$ are given in terms of their initial conditions evaluated at μ_0 by

$$\begin{aligned}
C_{S,AL}(\mu_1) &= \eta^{-4/\beta_s}\, C_{S,AL}(\mu_0)\,, \\
C_{V,AL}(\mu_1) &= C_{V,AL}(\mu_0)\,, \\
C_{T,A}(\mu_1) &= \eta^{4/(3\,\beta_s)}\, C_{T,A}(\mu_0)\,, \\
C_{7,A}(\mu_1) &= \eta^{4/(3\,\beta_s)-1}\, C_{7,A}(\mu_0) + \frac{4}{\beta_s}\left(1-\eta^{-1}\right)\eta^{4/(3\,\beta_s)}\, C_{T,A}(\mu_0)\,, \\
C_{9,A}(\mu_1) &= \eta^{-1}\, C_{9,A}(\mu_0) + \frac{2}{3\beta_s}\left(1-\eta^{-1}\right)\,\left(C_{V,AL}(\mu_0) + C_{V,AR}(\mu_0)\right)\,,
\end{aligned} \tag{A2}$$

where $\eta = \alpha_s(\mu_0)/\alpha_s(\mu_1)$. These results hold if one does not cross a quark threshold in between μ_0 and μ_1. Generalizing them to include threshold effects is however straightforward, since the evolution factorizes and finite matching corrections are not present at LO.

B Kinematic Functions

In this appendix, we collect the analytic results for the functions $M_i^{X_s}(s)$ and $M_i^{K^+}(s)$, which appear in the formulas (36) and (41) for the differential branching ratios of the $B \to X_s\tau^+\tau^-$ and $B \to K^+\tau^+\tau^-$ decays.

In the case of the inclusive $b \to s\tau^+\tau^-$ transition, the relevant kinematic functions are given by the following expressions [51]

$$\begin{aligned}
M_S^{X_s}(s) &= 2s\left(1-\frac{2m_\tau^2}{s}\right)\left(m_b^2+m_s^2-s\right) g_{X_s}(s)\,, \\
M_V^{X_s}(s) &= 2\left[\left(m_b^2-m_s^2\right)^2 - s^2 - \frac{g_{X_s}^2(s)}{3}\right] g_{X_s}(s)\,, \\
M_T^{X_s}(s) &= \frac{32}{3}\left(1+\frac{2m_\tau^2}{s}\right)\left[2\left(m_b^2-m_s^2\right)^2 - s\left(m_b^2+m_s^2+s\right)\right]\, g_{X_s}(s)\,,
\end{aligned} \tag{B1}$$

where

$$g_{X_s}(s) = \beta\,\sqrt{\lambda(s,m_b,m_s)}\,, \tag{B2}$$

and

$$\beta = \sqrt{1 - \frac{4m_\tau^2}{s}}\,, \qquad \lambda(a,b,c) = \left(a - (b+c)^2\right)\left(a - (b-c)^2\right)\,. \tag{B3}$$

In the case of the exclusive decay, the relevant expressions take instead the form [55]

$$\begin{aligned}
M_S^{K^+}(s) &= \frac{3}{16}\left(\frac{M_{B^+}^2 - M_{K^+}^2}{m_b - m_s}\right)^2 s\left(1 - \frac{2m_\tau^2}{s}\right) f_0^2(s)\, g_{K^+}(s)\,,\\
M_V^{K^+}(s) &= \frac{1}{8s}\left[3m_\tau^2\left(M_{B^+}^2 - M_{K^+}^2\right)^2 f_0^2(s) + \lambda(s, M_{B^+}, M_{K^+})\,(s - m_\tau^2)\, f_+^2(s)\right] g_{K^+}(s)\,,\\
M_T^{K^+}(s) &= \frac{s}{(M_{B^+} + M_{K^+})^2}\left(1 + \frac{2m_\tau^2}{s}\right)\lambda(s, M_{B^+}, M_{K^+})\, f_T^2(s)\, g_{K^+}(s)\,,
\end{aligned} \tag{B4}$$

with

$$g_{K^+}(s) = \beta\,\sqrt{\lambda(s, M_{B^+}, M_{K^+})}\,, \tag{B5}$$

and $M_{K^+} = 493.677$ MeV [38]. The s-dependence of the $B^+ \to K^+$ form factors $f_i(s)$ entering (B4) is modeled using the results obtained in [111]. Explicitly, we employ ($\bar{s} = s/\text{GeV}^2$)

$$\begin{aligned}
f_+(s) &= \left(-5.6314 + 6.9718\,\sqrt{33.3258 - \bar{s}} + 0.6206\,\bar{s}\right) d_1(\bar{s})\, d_2(\bar{s})\,,\\
f_T(s) &= \left(-7.7322 + 8.2175\,\sqrt{33.3258 - \bar{s}} + 0.7643\,\bar{s}\right) d_1(\bar{s})\, d_2(\bar{s})\,,\\
f_0(s) &= \left(-30.040 + 11.200\,\sqrt{33.3258 - \bar{s}} + 1.6269\,\bar{s}\right) d_2(\bar{s})\,,
\end{aligned} \tag{B6}$$

with $d_1(\bar{s}) = (1 - \bar{s}/M_{B_s^*(1^-)}^2)^{-1}$, $d_2(\bar{s}) = \left(4.3173 + \sqrt{33.3258 - \bar{s}}\right)^{-2}$, and $M_{B_s^*(1^-)} = 5.412$ GeV.

C Matrix Elements for $b \to s\ell^+\ell^-$

This appendix contains the analytic results for the $b \to s\ell^+\ell^-$ matrix elements of the complete set of $(\bar{s}b)(\bar{\tau}\tau)$ operators

$$Q_i = (\bar{s}\,\Gamma_{\bar{s}b}^i\, b)(\bar{\tau}\,\Gamma_{\bar{\tau}\tau}^i\,\tau)\,, \tag{C1}$$

with $\Gamma_{\bar{s}b}^i \otimes \Gamma_{\bar{\tau}\tau}^i = \{P_A \otimes P_B, \gamma^\mu P_A \otimes \gamma_\mu P_B, \sigma^{\mu\nu} P_A \otimes \sigma_{\mu\nu} P_A\}$. The diagram with the closed tau loop shown on the right-hand side in Figure 3 yields the following amplitude for the operator insertion

$$\begin{aligned}
\mathcal{A} = i\mathcal{N} Q_\tau\,(\bar{s}\,\Gamma_{\bar{s}b}^i\, b)(\bar{\ell}\,\gamma^\alpha\,\ell)\,\Bigg\{&\frac{m_\tau}{q^2}\left[\Delta + \ln x_\mu - \frac{1}{4}M_7(\hat{s}, x_\tau)\right]\text{Tr}\left[\gamma_\alpha \not{q}\,\Gamma_{\bar{\tau}\tau}^i\right]\\
&+\left[\frac{1}{3}\left(\Delta + \ln x_\mu\right) - \frac{1}{2}M_9(\hat{s}, x_\tau)\right]\text{Tr}\left[\gamma_\alpha \Gamma_{\bar{\tau}\tau}^i\right]\Bigg\}\, C_i\,.
\end{aligned} \tag{C2}$$

Here C_i is the relevant Wilson coefficient and

$$\mathcal{N} = \frac{4G_F}{\sqrt{2}}\,\frac{\alpha}{4\pi}\,V_{ts}^* V_{tb}\,, \qquad \Delta = \frac{1}{\varepsilon} - \gamma_E + \ln(4\pi)\,, \qquad x_\mu = \frac{\mu^2}{m_b^2}\,, \tag{C3}$$

and $\gamma_E \approx 0.577216$ denotes the Euler-Mascheroni constant. The functions $M_7(\hat{s}, x_\tau)$ and $M_9(\hat{s}, x_\tau)$ entering (C2) are given by

$$\begin{aligned} M_7(\hat{s}, x_\tau) &= -8 + 4\ln x_\tau + 4\, g(y)\,, \\ M_7(0, x_\tau) &= 4\ln x_\tau\,, \end{aligned} \tag{C4}$$

and

$$\begin{aligned} M_9(\hat{s}, x_\tau) &= -\frac{2}{9}\,(5+3y) + \frac{2}{3}\ln x_\tau + \frac{1}{3}\,(2+y)\, g(y)\,, \\ M_9(\hat{s}, 0) &= \frac{2}{3}\,(\ln\hat{s} - i\pi) - \frac{10}{9}\,, \end{aligned} \tag{C5}$$

where $y = 4m_\tau^2/s$ and

$$g(y) = \sqrt{|1-y|}\,\begin{cases} \left[\ln\left(\dfrac{1+\sqrt{1-y}}{1-\sqrt{1-y}}\right) - i\pi\right], & y < 1\,, \\ 2\tan^{-1}\left(\dfrac{1}{\sqrt{y-1}}\right), & y > 1\,. \end{cases} \tag{C6}$$

The terms $\mathrm{Tr}\,[\gamma_\alpha \not{q}\, \Gamma^i_{\bar{\tau}\tau}]$ and $\mathrm{Tr}\,[\gamma_\alpha \Gamma^i_{\bar{\tau}\tau}]$ in (C2) give rise to the contributions proportional to the electromagnetic dipole operators $Q_{7,A}$ and the vector-like semileptonic operators $Q_{9,A}$, respectively. The relevant non-zero Dirac traces are

$$\mathrm{Tr}\,[\gamma_\alpha \not{q} P_A] = 2q_\alpha\,, \quad \mathrm{Tr}\,[\gamma_\alpha \gamma_\mu P_A] = 2g_{\alpha\mu}\,, \quad \mathrm{Tr}\,[\gamma_\alpha \not{q} \sigma_{\mu\nu} P_A] = 4i\,(q_\mu g_{\alpha\nu} - q_\nu g_{\alpha\mu})\,. \tag{C7}$$

Finally, the tree-level $b \to s\ell^+\ell^-$ matrix elements involving the operators (45) read

$$\begin{aligned} \langle Q_{7,A}\rangle_{\text{tree}} &= i\mathcal{N}\, 2\,\frac{m_\tau}{q^2}(\bar{s}\,\gamma^\mu \not{q} P_A\, b)(\bar{\ell}\,\gamma_\mu\,\ell)\,, \\ \langle Q_{9,A}\rangle_{\text{tree}} &= i\mathcal{N}\,(\bar{s}\,\gamma^\mu P_A\, b)(\bar{\ell}\,\gamma_\mu \ell)\,. \end{aligned} \tag{C8}$$

By combining (C2), (C7), and (C8) it is a matter of simple algebra to derive both the expressions given in (47) as well as the relevant entries of the LO ADM in (A1).

D Matrix Elements for $b \to s\gamma\gamma$

In the following, we present the analytic results for the one-loop matrix elements involving an insertion of a $(\bar{s}b)(\bar{\tau}\tau)$ operator, which enter the LO prediction for $B_s \to \gamma\gamma$. The relevant decay amplitude has the following general structure

$$\begin{aligned} \mathcal{A} &= \frac{\mathcal{N}}{3}\,\frac{f_{B_s}}{2}\,\langle\gamma\gamma|A_+\, F_{\mu\nu}F^{\mu\nu} - iA_-\, F_{\mu\nu}\tilde{F}^{\mu\nu}|0\rangle \\ &= \frac{\mathcal{N}}{3}\, f_{B_s}\left\{A_+\left(2k_1\cdot\varepsilon_2\, k_2\cdot\varepsilon_1 - M_{B_s}^2\,\varepsilon_1\cdot\varepsilon_2\right) - 2iA_-\,\epsilon(k_1,k_2,\varepsilon_1,\varepsilon_2)\right\} \end{aligned} \tag{D1}$$

where $\mathcal{N}$ has been defined in (C3), $F_{\mu\nu}$ and $\tilde{F}_{\mu\nu} = \epsilon_{\mu\nu\lambda\rho}/2\, F^{\lambda\rho}$ are the photon field strength tensor and its dual, $k_{1,2}$ and $\varepsilon_{1,2}$ denote the momenta and the polarization vectors of the two photons, and we have introduced $\epsilon(a,b,c,d) = \epsilon_{\mu\nu\lambda\rho} a^\mu b^\nu c^\lambda d^\rho$. The subscripts $\pm$ on the coefficients $A_\pm$, denote the CP properties of the corresponding two-photon final state with A_+ (A_-) being proportional to the parallel (perpendicular) spin polarization $\vec{\varepsilon}_1 \cdot \vec{\varepsilon}_2$ ($\vec{\varepsilon}_1 \times \vec{\varepsilon}_2$).

We find that the non-vanishing matrix elements $\langle Q_i \rangle = \langle \gamma\gamma | Q_i | \bar{B}_s \rangle$ arising from operator insertions into the Feynman diagram of Figure 4, are given by ($y_\tau = m_\tau^2/M_{B_s}^2$)

$$\langle Q_{S,LA} \rangle = \frac{\alpha}{8\pi}\, f_{B_s}\, \frac{M_{B_s}}{m_\tau}\, Q_\tau^2 \left\{ \frac{1}{2} \left[2 + (1-4y_\tau)\, h(y_\tau) \right] \left(2k_1 \cdot \varepsilon_2\, k_2 \cdot \varepsilon_1 - M_{B_s}^2\, \varepsilon_1 \cdot \varepsilon_2 \right) \right.$$
$$\left. \mp \left[2 + h(y_\tau) \right] i\, \epsilon(k_1, k_2, \varepsilon_1, \varepsilon_2) \right\}, \tag{D2}$$

$$\langle Q_{V,LA} \rangle = \frac{\alpha}{4\pi}\, f_{B_s}\, Q_\tau^2 \left\{ \pm\, h(y_\tau)\, i\, \epsilon(k_1, k_2, \varepsilon_1, \varepsilon_2) \right\},$$

with

$$h(y) = -2 \left[1 + y \ln^2 \left(\frac{\sqrt{1-4y} - 1}{\sqrt{1-4y} + 1} \right) \right]. \tag{D3}$$

Here $\alpha = 1/137.036$ and the upper (lower) signs hold in the case $A = L$ ($A = R$). The expressions (D2) can be shown to resemble the results of [87, 90]. The formulas that apply in the case of $Q_{S,RA}$ and $Q_{V,RA}$ are obtained from (D2) by reversing the overall sign. Notice that although the 1PI diagrams with an insertion of a tensor operator with flavor content $(\bar{s}b)(\bar{\tau}\tau)$ evaluate to zero, the operators $Q_{T,A}$ contribute to the amplitude (D1), because the tensor operators lead to corrections $\Delta C_7^{(\prime)\text{eff}}$ to the effective Wilson coefficients of $Q_7^{(\prime)}$. We finally mention that $\langle Q_{S,AB} \rangle$ scales like the mass of the charged lepton in the loop. This implies that $\langle Q_{S,AB} \rangle \to 0$ for $y \to 0$, since $h(y) \to -2$ in this limit. The matrix elements of scalar operators involving electrons or muons are therefore to first approximation equal to zero. In the case of tau leptons the chiral suppression is compensated by the large logarithms $\ln y$ and the numerical factors appearing in $h(y) = -2 + \left(-2\ln^2 y + 2\pi^2 - 4i\pi \ln y \right) y + \mathcal{O}(y^2)$.

Combining (D1) and (D2) it follows that the new-physics corrections to the coefficients $A_\pm$ take the form

$$\begin{aligned} \Delta A_+ &= \frac{M_{B_s}}{\lambda_B} \left(\Delta C_7^{\text{eff}} - \Delta C_7^{\prime\text{eff}} \right) - \frac{3}{4}\, \frac{M_{B_s}}{m_\tau} \left[2 + (1-4y_\tau)\, h(y_\tau) \right] F_S^+ , \\ \Delta A_- &= \frac{M_{B_s}}{\lambda_B} \left(\Delta C_7^{\text{eff}} + \Delta C_7^{\prime\text{eff}} \right) - \frac{3}{4}\, \frac{M_{B_s}}{m_\tau} \left[2 + h(y_\tau) \right] F_S^- + \frac{3}{2}\, h(y_\tau)\, F_V^- , \end{aligned} \tag{D4}$$

where

$$F_i^\pm = C_{i,LL} \pm C_{i,LR} - C_{i,RL} \mp C_{i,RR}\,. \tag{D5}$$

Notice that only the contributions associated with $Q_7^{(\prime)}$ contribute to the $B_s \to \gamma\gamma$ amplitudes at leading power in Λ_{QCD}/m_b, while the effects arising from the $(\bar{s}b)(\bar{\tau}\tau)$ insertions are relative to the leading terms suppressed by one power of $\lambda_B/M_{B_s} = \mathcal{O}(\Lambda_{\text{QCD}}/m_b)$.

After summing over the photon polarizations the branching ratio of $B_s \to \gamma\gamma$ becomes

$$\mathcal{B}(B_s \to \gamma\gamma) = \frac{\mathcal{N}^2 M_{B_s}^3 f_{B_s}^2 \tau_{B_s}}{144\pi} \left(|(A_+)_{\rm SM} + \Delta A_+|^2 + |(A_-)_{\rm SM} + \Delta A_-|^2 \right), \tag{D6}$$

where $(A_\pm)_{\rm SM}$ denotes SM contributions to $A_\pm$. Explicit formulas for the SM coefficients, including leading as well as subleading corrections in $\Lambda_{\rm QCD}/m_b$, can be found in [89, 90].

E Forward-Scattering Amplitudes

In this appendix, we give some details on the calculation of the contributions from the complete set of operators (22) to Γ_{12}^s. Since the decay width is related to the absorptive part of the forward scattering amplitude, the off-diagonal element of the decay-width matrix may be written as

$$\Gamma_{12}^s = \frac{1}{2M_{B_s}} \langle \bar{B}_s | \mathcal{T} | B_s \rangle \,, \tag{E1}$$

with the transition operator $\mathcal{T}$ given by

$$\mathcal{T} = 8 G_F^2 \left(V_{ts}^* V_{tb}\right)^2 \sum_{i,j} \text{Im} \left\{ i \int d^4x \; T \left[C_i Q_i(x) \, C_j Q_j(0) \right] \right\} . \tag{E2}$$

Here T denotes time ordering, the Wilson coefficients C_i are normalized as in (19) and (23).

At leading power in $\Lambda_{\rm QCD}/m_b$ the contribution to Γ_{12}^s is found by computing the matrix elements of $\mathcal{T}$ between quark states. The corresponding Feynman diagram involving an insertion of a pair (i,j) of operators (C1) is depicted in Figure 5. Treating the external quarks as on-shell and neglecting the strange-quark mass, we obtain from the discontinuity of the graph

$$\begin{aligned} (\Gamma_{12}^s)_{ij} = -\frac{3}{2} \mathcal{N}_{\Gamma_{12}^s} C_i \, C_j \, \beta_\tau \Bigg\{ & x_\tau \, \text{Tr} \left[\Gamma^i_{\bar\tau\tau} \, \Gamma^j_{\bar\tau\tau} \right] + \frac{\sqrt{x_\tau}}{2m_b} \, \text{Tr} \left[\Gamma^i_{\bar\tau\tau} \left[\Gamma^j_{\bar\tau\tau}, \not{p}_b \right] \right] \\ & - \frac{1-4x_\tau}{12} \, \text{Tr} \left[\Gamma^i_{\bar\tau\tau} \gamma^\alpha \Gamma^j_{\bar\tau\tau} \gamma_\alpha \right] - \frac{1+2x_\tau}{6m_b^2} \, \text{Tr} \left[\Gamma^i_{\bar\tau\tau} \not{p}_b \Gamma^j_{\bar\tau\tau} \not{p}_b \right] \Bigg\} \langle \Gamma^i_{\bar s b} \, \Gamma^j_{\bar s b} \rangle \,, \end{aligned} \tag{E3}$$

with $\mathcal{N}_{\Gamma_{12}^s}$ and β_τ given in and before (61), respectively. Notice that the prefactor β_τ is related to the imaginary part of the Passarino-Veltman two-point integral $B_0(m_b^2, m_\tau^2, m_\tau^2)$. Explicitly, one has $\pi\beta_\tau = \text{Im}\left[B_0(m_b^2, m_\tau^2, m_\tau^2)\right]$. The result (E3) can be shown to agree with the general findings of [112, 113, 114].

The general result (E3) simplifies if one considers the self-interference of operators only. Due to the cyclicity of the trace one has $\text{Tr}\left[\Gamma^i_{\bar\tau\tau} \left[\Gamma^i_{\bar\tau\tau}, \not{p}_b\right]\right] = 0$ for all $i = S, AB, V, AB, T, A$. In the case of $i = S, AB, T, A$ the only non-vanishing Dirac traces read

$$\text{Tr}\left[P_{L,R} \, P_{L,R}\right] = 2 \,, \qquad \text{Tr}\left[\sigma^{\mu\nu} P_{L,R} \, \sigma^{\lambda\rho} P_{L,R}\right] = 2 \left(g^{\mu\lambda} g^{\nu\rho} - g^{\mu\rho} g^{\nu\lambda} \mp i\epsilon^{\mu\nu\lambda\rho} \right) , \tag{E4}$$

where the Levi-Civita Tensor $\epsilon^{\mu\nu\lambda\rho}$ is related to γ_5 via $\gamma_5 = -i/4!\, \epsilon^{\mu\nu\lambda\rho} \gamma_\mu\gamma_\nu\gamma_\lambda\gamma_\rho$. For $i = V, AB$ one needs instead

$$\text{Tr}\left[\gamma^\mu P_{L,R} \, \gamma^\alpha \, \gamma^\nu P_{L,R} \, \gamma_\alpha\right] = -4 g^{\mu\nu} \,, \qquad \text{Tr}\left[\gamma^\mu P_{L,R} \not{p}_b \, \gamma^\nu P_{L,R} \not{p}_b\right] = 2 \left(2 p_b^\mu p_b^\nu - m_b^2 g^{\mu\nu} \right) . \tag{E5}$$

In order to derive the expressions given in (60), one still has to take into account that

$$i\epsilon^{\mu\nu\lambda\rho}\,(\bar{s}\,\sigma_{\mu\nu}P_{L,R}\,b)\,(\bar{s}\,\sigma_{\lambda\rho}P_{L,R}\,b) = \mp 2\,(\bar{s}\,\sigma^{\mu\nu}P_{L,R}\,b)\,(\bar{s}\,\sigma_{\mu\nu}P_{L,R}\,b)\;, \tag{E6}$$

and apply the Fierz identity

$$(\bar{s}\,\sigma^{\mu\nu}P_{L,R}\,b)\,(\bar{s}\,\sigma_{\mu\nu}P_{L,R}\,b) = -4\,(\bar{s}\,P_{L,R}\,b)\,(\bar{s}\,P_{L,R}\,b) - 8\,(\bar{s}_\alpha\,P_{L,R}\,b_\beta)\,(\bar{s}_\beta\,P_{L,R}\,b_\alpha)\;. \tag{E7}$$

F Bounds on $\Delta\Gamma_s$ and a^s_{fs} from ΔM_s

In this appendix, we show that in the class of SM extensions with real $(M^s_{12})_{\rm NP}/(\Gamma^s_{12})_{\rm NP}$, a bound on ΔM_s necessarily results in a limit on both $\Delta\Gamma_s$ and a^s_{fs}. We start our derivation by noting that under the assumption that $\arg\left((M^s_{12})_{\rm NP}/(\Gamma^s_{12})_{\rm NP}\right)$ is either equal to 0° or 180°, the parameters $R_{M,\Gamma}$ introduced in (14) can be expressed in terms of the three ratios

$$r_M = \frac{(M^s_{12})_{\rm NP}}{(M^s_{12})_{\rm SM}}\,, \qquad r_{\rm SM} = \frac{(M^s_{12})_{\rm SM}}{(\Gamma^s_{12})_{\rm SM}}\,, \qquad r_{\rm NP} = \frac{(M^s_{12})_{\rm NP}}{(\Gamma^s_{12})_{\rm NP}}\,, \tag{F1}$$

and $\phi^s_{\rm SM}$, as follows

$$R_M = |1 + r_M|\,, \qquad R_\Gamma = \left|1 - {\rm sgn}\,(r_{\rm NP})\,\frac{|r_{\rm SM}|}{|r_{\rm NP}|}\,r_M\,e^{i\phi^s_{\rm SM}}\right| \approx \left|1 - {\rm sgn}\,(r_{\rm NP})\,\frac{|r_{\rm SM}|}{|r_{\rm NP}|}\,r_M\right|\,. \tag{F2}$$

Because $\phi^s_{\rm SM}$ is only a fraction of 1°, the approximation made to obtain the final expression for R_Γ is sufficient for all practical purposes.

In order to simplify the further discussion, we consider the two possible signs of $r_{\rm NP}$ separately. We begin with ${\rm sgn}\,(r_{\rm NP}) = +1$. From (F2) it is readily seen that in this case, the value of R_Γ becomes maximal (minimal) if r_M is real, negative (positive), and as large as possible in magnitude. A two-sided bound on ΔM_s or equivalently R_M,

$$R_M^{\rm min} < R_M < R_M^{\rm max}\,, \tag{F3}$$

with $R_M^{\rm min} < 1$ and $R_M^{\rm max} > 1$,[19] thus constrains the possible values of R_Γ to lie in the interval

$$\max\left(0, 1 - \left(R_M^{\rm max} - 1\right)\frac{|r_{\rm SM}|}{|r_{\rm NP}|}\right) < R_\Gamma < 1 + \left(R_M^{\rm max} + 1\right)\frac{|r_{\rm SM}|}{|r_{\rm NP}|}\,. \tag{F4}$$

According to (15) a bound on R_Γ also restricts the allowed range for $\Delta\Gamma_s$. Since one has $\phi_M = 180^\circ$ and $\phi_\Gamma = 0^\circ$ if R_Γ becomes maximal, the upper limit in (F4) leads to a lower bound on $\Delta\Gamma_s$. On the other hand, the upper limit on $\Delta\Gamma_s$ arises if $\phi_M = \phi_\Gamma = 0^\circ$ and $r_M = R_M^{\rm min} - 1 < R_M^{\rm max} - 1$. One therefore has

$$-\left[1 + (R_M^{\rm max} + 1)\,\frac{|r_{\rm SM}|}{|r_{\rm NP}|}\right](\Delta\Gamma_s)_{\rm SM} < (\Delta\Gamma_s)_{\rm NP} < \left[1 - (R_M^{\rm min} - 1)\,\frac{|r_{\rm SM}|}{|r_{\rm NP}|}\right](\Delta\Gamma_s)_{\rm SM}\,. \tag{F5}$$

[19] This is the relevant case in view of the good agreement between $(\Delta M_s)_{\rm SM}$ and measured value of the mass difference. It is straightforward to extend the given formulas to the other possible cases.

Given that both R_M and R_Γ are bounded it is not surprising that also a^s_{fs} satisfies a double inequality. Because the expression (15) for a^s_{fs} is inversely proportional to R_M, the CP asymmetry becomes extremal for $R_M = R_M^{\rm min}$. It is then easy to convince oneself, that for this value of R_M the combination of $R_\Gamma \sin(\phi_M - \phi_\Gamma)$ is maximized/minimized if r_M is purely imaginary, corresponding to $\phi_M = \pm 90°$. After some algebraic simplifications, one arrives at

$$-\frac{1}{R_M^{\rm min}}\left[1+\frac{|r_{\rm SM}|}{|r_{\rm NP}|}\right]\frac{(a^s_{fs})_{\rm SM}}{\phi^s_{\rm SM}} < (a^s_{fs})_{\rm NP} < \frac{1}{R_M^{\rm min}}\left[1+\frac{|r_{\rm SM}|}{|r_{\rm NP}|}\right]\frac{(a^s_{fs})_{\rm SM}}{\phi^s_{\rm SM}}\,. \tag{F6}$$

Using the same line of reasoning as above, it is also not too difficult to derive the constraints for $\mathrm{sgn}(r_{\rm NP}) = -1$ that follow from (F3) with $R_M^{\rm min} < 1$ and $R_M^{\rm max} > 1$. One has to differentiate between the case $|r_{\rm SM}|/|r_{\rm NP}| < 1$ and $|r_{\rm SM}|/|r_{\rm NP}| > 1$. In the former case, we obtain

$$\begin{aligned}
&\max\left(0, 1-\left(R_M^{\rm max}+1\right)\frac{|r_{\rm SM}|}{|r_{\rm NP}|}\right) < R_\Gamma < 1+\left(R_M^{\rm max}-1\right)\frac{|r_{\rm SM}|}{|r_{\rm NP}|}\,,\\
&\left[-1+\left(R_M^{\rm min}+1\right)\frac{|r_{\rm SM}|}{|r_{\rm NP}|}\right](\Delta\Gamma_s)_{\rm SM} < (\Delta\Gamma_s)_{\rm NP} < \left[1+\left(R_M^{\rm max}-1\right)\frac{|r_{\rm SM}|}{|r_{\rm NP}|}\right](\Delta\Gamma_s)_{\rm SM}\,,
\end{aligned} \tag{F7}$$

while in the latter case the relations

$$\begin{aligned}
&\max\left(0, 1+\left(R_M^{\rm min}-1\right)\frac{|r_{\rm SM}|}{|r_{\rm NP}|}\right) < R_\Gamma < -1+\left(R_M^{\rm max}+1\right)\frac{|r_{\rm SM}|}{|r_{\rm NP}|}\,,\\
&\left[1+\left(R_M^{\rm min}-1\right)\frac{|r_{\rm SM}|}{|r_{\rm NP}|}\right](\Delta\Gamma_s)_{\rm SM} < (\Delta\Gamma_s)_{\rm NP} < \left[-1+\left(R_M^{\rm max}+1\right)\frac{|r_{\rm SM}|}{|r_{\rm NP}|}\right](\Delta\Gamma_s)_{\rm SM}\,,
\end{aligned} \tag{F8}$$

apply. The constraint on the CP asymmetry is independent of whether $|r_{\rm SM}|/|r_{\rm NP}|$ is smaller or bigger than 1. It takes the simple form

$$-\frac{1}{R_M^{\rm min}}\left|1-\frac{|r_{\rm SM}|}{|r_{\rm NP}|}\right|\frac{(a^s_{fs})_{\rm SM}}{\phi^s_{\rm SM}} < (a^s_{fs})_{\rm NP} < \frac{1}{R_M^{\rm min}}\left|1-\frac{|r_{\rm SM}|}{|r_{\rm NP}|}\right|\frac{(a^s_{fs})_{\rm SM}}{\phi^s_{\rm SM}}\,. \tag{F9}$$

The formulas (F4) to (F9) have a couple of features that are worth mentioning. First, the possible variations increase with decreasing $|r_{\rm SM}|/|r_{\rm NP}|$. Second, the limits on $\Delta\Gamma_s$ and a^s_{fs} are less stringent if $\mathrm{sgn}(r_{\rm NP}) = +1$. The only exception is the upper bound on $\Delta\Gamma_s$, which becomes weakest for $\mathrm{sgn}(r_{\rm NP}) = -1$ and $|r_{\rm SM}|/|r_{\rm NP}| > 1$. In new-physics scenarios with real $(M^s_{12})_{\rm NP}/(\Gamma^s_{12})_{\rm NP}$, non-standard effects in $\Delta\Gamma_s$ and a^s_{fs} are hence the least constrained by the measurement of ΔM_s, if the ratio $r_{\rm SM}/r_{\rm NP}$ is positive and as small as possible.

References

[1] A. Abulencia *et al.* [CDF Collaboration], Phys. Rev. Lett. **97**, 242003 (2006) [arXiv:hep-ex/0609040].

[2] LHCb Collaboration, LHCb-CONF-2011-050.

[3] A. Lenz and U. Nierste, arXiv:1102.4274 [hep-ph].

[4] T. Aaltonen *et al.* [CDF Collaboration], Phys. Rev. Lett. **100**, 161802 (2008) [arXiv:0712.2397 [hep-ex]].

[5] T. Aaltonen *et al.* [CDF collaboration], Phys. Rev. Lett. **100**, 121803 (2008) [arXiv:0712.2348 [hep-ex]].

[6] DØ Collaboration, Conference Note 5933-CONF, May 28, 2009, http://www-d0.fnal.gov/Run2Physics/WWW/results/prelim/B/B58/B58.pdf

[7] D. Asner *et al.* [Heavy Flavor Averaging Group], arXiv:1010.1589 [hep-ex], updated results available at `http://www.slac.stanford.edu/xorg/hfag/`

[8] R. Aaij *et al.* [LHCb Collaboration], Phys. Rev. Lett. **108**, 241801 (2012) [arXiv:1202.4717 [hep-ex]].

[9] A. Lenz *et al.*, Phys. Rev. D **83**, 036004 (2011) [arXiv:1008.1593 [hep-ph]].

[10] A. Lenz, Phys. Rev. D **84**, 031501 (2011) [arXiv:1106.3200 [hep-ph]].

[11] Y. Amhis *et al.* [Heavy Flavor Averaging Group Collaboration], arXiv:1207.1158 [hep-ex].

[12] [CDF Collaboration], Phys. Rev. Lett. **109**, 171802 (2012) [arXiv:1208.2967 [hep-ex]].

[13] V. M. Abazov *et al.* [DØ Collaboration], Phys. Rev. D **85**, 032006 (2012) [arXiv:1109.3166 [hep-ex]].

[14] LHCb Collaboration, LHCb note CERN-LHCb-CONF-2012-002, March 5, 2012, http://cdsweb.cern.ch/record/1423592

[15] R. Aaij *et al.* [LHCb Collaboration], Phys. Lett. B **713**, 378 (2012) [arXiv:1204.5675 [hep-ex]].

[16] G. Aad *et al.* [ATLAS Collaboration], arXiv:1208.0572 [hep-ex].

[17] V. M. Abazov *et al.* [DØ Collaboration], Phys. Rev. D **86**, 072009 (2012) [arXiv:1208.5813 [hep-ex]].

[18] CDF Collaboration, CDF Note 9015, October 16, 2007, http://www-cdf.fnal.gov/physics/new/bottom/070816.blessed-acp-bsemil/public-acp-bsemil.ps

[19] V. M. Abazov *et al.* [DØ Collaboration], Phys. Rev. D **82**, 032001 (2010) [arXiv:1005.2757 [hep-ex]].

[20] V. M. Abazov *et al.* [DØ Collaboration], Phys. Rev. Lett. **105**, 081801 (2010) [arXiv:1007.0395 [hep-ex]].

[21] V. M. Abazov *et al.* [DØ Collaboration], Phys. Rev. D **84**, 052007 (2011) [arXiv:1106.6308 [hep-ex]].

[22] LHCb Collaboration, LHCb-CONF-2012-022.

[23] A. Dighe, A. Kundu and S. Nandi, Phys. Rev. D **82**, 031502 (2010) [arXiv:1005.4051 [hep-ph]].

[24] B. A. Dobrescu, P. J. Fox and A. Martin, Phys. Rev. Lett. **105**, 041801 (2010) [arXiv:1005.4238 [hep-ph]].

[25] Z. Ligeti, M. Papucci, G. Perez and J. Zupan, Phys. Rev. Lett. **105**, 131601 (2010) [arXiv:1006.0432 [hep-ph]].

[26] C. W. Bauer and N. D. Dunn, Phys. Lett. B **696**, 362 (2011) [arXiv:1006.1629 [hep-ph]].

[27] Y. Bai and A. E. Nelson, Phys. Rev. D **82**, 114027 (2010) [arXiv:1007.0596 [hep-ph]].

[28] S. Oh and J. Tandean, Phys. Lett. B **697**, 41 (2011) [arXiv:1008.2153 [hep-ph]].

[29] A. K. Alok, S. Baek and D. London, JHEP **1107**, 111 (2011) [arXiv:1010.1333 [hep-ph]].

[30] J. E. Kim, M. S. Seo and S. Shin, Phys. Rev. D **83**, 036003 (2011) [arXiv:1010.5123 [hep-ph]].

[31] S. Oh and J. Tandean, Phys. Rev. D **83**, 095006 (2011) [arXiv:1102.1680 [hep-ph]].

[32] B. Dutta, S. Khalil, Y. Mimura and Q. Shafi, JHEP **1205**, 131 (2012) [arXiv:1104.5209 [hep-ph]].

[33] A. Dighe, D. Ghosh, A. Kundu and S. K. Patra, Phys. Rev. D **84**, 056008 (2011) [arXiv:1105.0970 [hep-ph]].

[34] F. Goertz and T. Pfoh, Phys. Rev. D **84**, 095016 (2011) [arXiv:1105.1507 [hep-ph]].

[35] A. Dighe, A. Kundu and S. Nandi, Phys. Rev. D **76**, 054005 (2007) [arXiv:0705.4547 [hep-ph]].

[36] M. Carpentier and S. Davidson, Eur. Phys. J. C **70**, 1071 (2010) [arXiv:1008.0280 [hep-ph]].

[37] Y. Grossman, Z. Ligeti and E. Nardi, Phys. Rev. D **55**, 2768 (1997) [arXiv:hep-ph/9607473].

[38] K. Nakamura *et al.* [Particle Data Group], J. Phys. G **37**, 075021 (2010), updated results available at `http://pdglive.lbl.gov`

[39] A. Lenz, U. Nierste and G. Ostermaier, Phys. Rev. D **56**, 7228 (1997) [arXiv:hep-ph/9706501].

[40] E. Bagan, P. Ball, V. M. Braun and P. Gosdzinsky, Phys. Lett. B **342**, 362 (1995) [Erratum-ibid. B **374**, 363 (1996)] [hep-ph/9409440].

[41] M. Neubert and C. T. Sachrajda, Nucl. Phys. B **483**, 339 (1997) [hep-ph/9603202].

[42] A. L. Kagan and J. Rathsman, arXiv:hep-ph/9701300.

[43] A. Kagan, arXiv:hep-ph/9806266.

[44] B. Aubert *et al.* [BaBar Collaboration], Phys. Rev. D **75**, 072002 (2007) [arXiv:hep-ex/0606026].

[45] P. Abreu *et al.* [DELPHI Collaboration], Phys. Lett. **B426**, 193-206 (1998).

[46] K. Flood [BaBar Collaboration], PoS **ICHEP2010**, 234 (2010).

[47] C. Bobeth, T. Ewerth, F. Krüger and J. Urban, Phys. Rev. D **66**, 074021 (2002) [arXiv:hep-ph/0204225].

[48] J. Laiho, E. Lunghi and R. S. Van de Water, Phys. Rev. D **81**, 034503 (2010) [arXiv:0910.2928 [hep-ph]].

[49] J. Charles *et al.* [CKMfitter Group], Eur. Phys. J. C **41**, 1 (2005) [arXiv:hep-ph/0406184], updated results available at `http://ckmfitter.in2p3.fr`

[50] C. Bobeth, P. Gambino, M. Gorbahn and U. Haisch, JHEP **0404**, 071 (2004) [arXiv:hep-ph/0312090].

[51] S. Fukae, C. S. Kim, T. Morozumi and T. Yoshikawa, Phys. Rev. D **59**, 074013 (1999) [arXiv:hep-ph/9807254].

[52] Y. Nir, Phys. Lett. B **221**, 184 (1989).

[53] J. L. Hewett, Phys. Rev. D **53**, 4964 (1996) [arXiv:hep-ph/9506289].

[54] D. S. Du, C. Liu and D. X. Zhang, Phys. Lett. B **317**, 179 (1993).

[55] C. Bobeth, G. Hiller and G. Piranishvili, JHEP **0712**, 040 (2007) [arXiv:0709.4174 [hep-ph]].

[56] F. Borzumati, C. Greub, T. Hurth and D. Wyler, Phys. Rev. D **62**, 075005 (2000) [arXiv:hep-ph/9911245].

[57] G. Hiller and F. Krüger, Phys. Rev. D **69**, 074020 (2004) [arXiv:hep-ph/0310219].

[58] A. J. Buras, M. Misiak, M. Münz and S. Pokorski, Nucl. Phys. B **424**, 374 (1994) [arXiv:hep-ph/9311345].

[59] M. Misiak *et al.*, Phys. Rev. Lett. **98**, 022002 (2007) [arXiv:hep-ph/0609232].

[60] M. Misiak and M. Steinhauser, Nucl. Phys. B **764**, 62 (2007) [arXiv:hep-ph/0609241].

[61] H. M. Asatrian,T. Ewerth, H. Gabrielyan and C. Greub, Phys. Lett. B **647**, 173 (2007) [arXiv:hep-ph/0611123].

[62] R. Boughezal, M. Czakon and T. Schutzmeier, JHEP **0709**, 072 (2007) [arXiv:0707.3090 [hep-ph]].

[63] T. Ewerth, Phys. Lett. B **669**, 167 (2008) [arXiv:0805.3911 [hep-ph]].

[64] H. M. Asatrian, T. Ewerth, A. Ferroglia, C. Greub and G. Ossola, Phys. Rev. D **82**, 074006 (2010) [arXiv:1005.5587 [hep-ph]].

[65] A. Ferroglia and U. Haisch, Phys. Rev. D **82**, 094012 (2010) [arXiv:1009.2144 [hep-ph]].

[66] M. Misiak and M. Poradzinski, Phys. Rev. D **83**, 014024 (2011) [arXiv:1009.5685 [hep-ph]].

[67] M. Czakon, U. Haisch and M. Misiak, JHEP **0703**, 008 (2007) [arXiv:hep-ph/0612329].

[68] P. Gambino, U. Haisch and M. Misiak, Phys. Rev. Lett. **94**, 061803 (2005) [arXiv:hep-ph/0410155].

[69] C. Bobeth, G. Hiller and G. Piranishvili, JHEP **0807**, 106 (2008) [arXiv:0805.2525 [hep-ph]].

[70] S. Descotes-Genon, D. Ghosh, J. Matias and M. Ramon, JHEP **1106**, 099 (2011) [arXiv:1104.3342 [hep-ph]].

[71] B. Aubert *et al.* [BaBar Collaboration], Phys. Rev. Lett. **93**, 081802 (2004) [arXiv:hep-ex/0404006].

[72] M. Iwasaki *et al.* [Belle Collaboration], Phys. Rev. D **72**, 092005 (2005) [arXiv:hep-ex/0503044].

[73] H. Nakayama, "Precision measurement of the electroweak flavor-changing neutral current decays of B mesons,", Ph. D. thesis, University of Tokyo, http://belle.kek.jp/belle/theses/doctor/2009/Nakayama.pdf

[74] C. C. Chiang [Belle Collaboration], PoS **ICHEP2010**, 231 (2010).

[75] B. Aubert *et al.* [BaBar Collaboration], Phys. Rev. D **73**, 092001 (2006) [arXiv:hep-ex/0604007].

[76] B. Aubert *et al.* [BaBar Collaboration], Phys. Rev. D **79**, 031102 (2009) [arXiv:0804.4412 [hep-ex]].

[77] J. T. Wei *et al.* [Belle Collaboration], Phys. Rev. Lett. **103**, 171801 (2009) [arXiv:0904.0770 [hep-ex]].

[78] T. Aaltonen *et al.* [CDF Collaboration], Phys. Rev. Lett. **106**, 161801 (2011) [arXiv:1101.1028 [hep-ex]].

[79] T. Aaltonen *et al.* [CDF Collaboration], Phys. Rev. Lett. **107**, 201802 (2011) [arXiv:1107.3753 [hep-ex]].

[80] LHCb Collaboration, LHCb-CONF-2011-038, August 10, 2011, http://cdsweb.cern.ch/record/1367849/files/LHCb-CONF-2011-038.pdf

[81] T. Aaltonen *et al.* [CDF Collaboration], Phys. Rev. Lett. **108**, 081807 (2012) [arXiv:1108.0695 [hep-ex]].

[82] M. Bauer, S. Casagrande, U. Haisch and M. Neubert, JHEP **1009**, 017 (2010) [arXiv:0912.1625 [hep-ph]].

[83] C. Bobeth, G. Hiller and D. van Dyk, JHEP **1007**, 098 (2010) [arXiv:1006.5013 [hep-ph]].

[84] C. Bobeth, G. Hiller and D. van Dyk, JHEP **1107**, 067 (2011) [arXiv:1105.0376 [hep-ph]].

[85] EOS Collaboration, "EOS: A HEP Program for Flavor Observables", http://project.het.physik.tu-dortmund.de/eos/

[86] A. Gemintern, S. Bar-Shalom and G. Eilam, Phys. Rev. D **70**, 035008 (2004) [arXiv:hep-ph/0404152].

[87] G. Hiller and A. S. Safir, JHEP **0502**, 011 (2005) [arXiv:hep-ph/0411344v4].

[88] J. Wicht *et al.* [Belle Collaboration], Phys. Rev. Lett. **100**, 121801 (2008) [arXiv:0712.2659 [hep-ex]].

[89] S. W. Bosch and G. Buchalla, JHEP **0208**, 054 (2002) [hep-ph/0208202].

[90] S. W. Bosch, [hep-ph/0208203].

[91] A. G. Grozin and M. Neubert, Phys. Rev. **D55**, 272-290 (1997) [hep-ph/9607366].

[92] P. Ball and E. Kou, JHEP **0304**, 029 (2003) [hep-ph/0301135].

[93] V. M. Braun, D. Y. Ivanov and G. P. Korchemsky, Phys. Rev. **D69**, 034014 (2004) [hep-ph/0309330].

[94] S. J. Lee and M. Neubert, Phys. Rev. **D72**, 094028 (2005) [hep-ph/0509350].

[95] T. Abe *et al.*, [hep-ph/0503261].

[96] D. Becirevic, V. Gimenez, G. Martinelli, M. Papinutto and J. Reyes, JHEP **0204**, 025 (2002) [arXiv:hep-lat/0110091].

[97] W. Buchmüller, R. Rückl and D. Wyler, Phys. Lett. B **191**, 442 (1987) [Erratum-ibid. B **448**, 320 (1999)].

[98] M. Leurer, Phys. Rev. D **49**, 333 (1994) [arXiv:hep-ph/9309266].

[99] S. Davidson, D. C. Bailey and B. A. Campbell, Z. Phys. C **61**, 613 (1994) [arXiv:hep-ph/9309310].

[100] J. L. Hewett and T. G. Rizzo, Phys. Rev. D **56**, 5709 (1997) [arXiv:hep-ph/9703337].

[101] V. M. Abazov *et al.* [DØ Collaboration], Phys. Rev. Lett. **101**, 241802 (2008) [arXiv:0806.3527 [hep-ex]].

[102] I. Dorsner, J. Drobnak, S. Fajfer, J. F. Kamenik and N. Kosnik, arXiv:1107.5393 [hep-ph].

[103] P. Langacker and M. Plümacher, Phys. Rev. D **62**, 013006 (2000) [arXiv:hep-ph/0001204].

[104] P. Langacker, Rev. Mod. Phys. **81**, 1199 (2009) [arXiv:0801.1345 [hep-ph]].

[105] X. G. He and G. Valencia, Phys. Rev. D **74**, 013011 (2006) [arXiv:hep-ph/0605202].

[106] D. E. Acosta *et al.* [CDF Collaboration], Phys. Rev. Lett. **95**, 131801 (2005) [arXiv:hep-ex/0506034].

[107] S. Schael *et al.* [ALEPH Collaboration], Phys. Rept. **427**, 257 (2006) [arXiv:hep-ex/0509008].

[108] U. Haisch and S. Westhoff, JHEP **1108**, 088 (2011) [arXiv:1106.0529 [hep-ph]].

[109] B. Aubert *et al.* [BaBar Collaboration], Phys. Rev. Lett. **99**, 201801 (2007) [arXiv:0708.1303 [hep-ex]].

[110] B. Aubert *et al.* [BABAR Collaboration], Phys. Rev. Lett. **96**, 241802 (2006) [hep-ex/0511015].

[111] A. Khodjamirian, T. Mannel, A. A. Pivovarov and Y. M. Wang, JHEP **1009**, 089 (2010) [arXiv:1006.4945 [hep-ph]].

[112] E. Golowich, S. Pakvasa and A. A. Petrov, Phys. Rev. Lett. **98**, 181801 (2007) [arXiv:hep-ph/0610039].

[113] S. L. Chen, X. G. He, A. Hovhannisyan and H. C. Tsai, JHEP **0709**, 044 (2007) [arXiv:0706.1100 [hep-ph]].

[114] A. Badin, F. Gabbiani and A. A. Petrov, Phys. Lett. B **653**, 230 (2007) [arXiv:0707.0294 [hep-ph]].